alla mia famiglia

Contents

List of Figures

List of Tables

Ringraziamenti

E' stato un percorso lungo e a volte complicato quello che mi ha portato fin qui ora, e non sarebbe stato possibile senza l'incondizionato appoggio che fin dall'inizio ho ricevuto da mio padre Lorenzo, da mia sorella Giulia e, sono sicuro, da mia madre Valeria che da lassù non ha mai smesso di credere in me. E' a loro che va il mio ringraziamento più grande.

Ai miei nonni, Giuseppe e Cesarina, per l'affetto e l'aiuto che non mi hanno mai fatto mancare.

Un ringraziamento speciale va poi a Federica, per la pazienza che da sempre ha avuto con me e per i suoi incoraggiamenti ad andare sempre avanti, a non mollare mai anche quando tutto era più grigio, più insicuro.

Un ringraziamento a tutti i miei amici, in particolare Luca, Chiara, Giulio e Jon che mi sono rimasti sempre vicino in questi anni.

Introduction

The synthetic aperture radar principle has been discovered in the early 50th. Since then, a rapid development took place all over the world. Today, synthetic aperture radar (SAR) plays an important role in military applications and earth observation. SAR systems offer advantages compared to competing sensors in infrared or visible spectral area, because of its day-and-night capability and the possibility to penetrate clouds and rain. Typical applications of SAR in the earth observation are for example topographic mapping (2D and 3D), surface movements detection, vegetation monitoring. One application currently under evaluation is the use of spaceborne SAR for traffic monitoring and maritime surveillance, and is in this field of application that this thesis gives its contribute. The maritime surveillance could be of help to prevent for example the illegal immigration phenomena that is affecting nowadays the southern Europe or can be used in piracy and illegal traffics (arms, toxic waste, etc) prevention. The European community has showed interest in this topic and has funded the NEWA (New EuropeanWAtcher) project in order to investigate the problem of the detection of moving targets using spaceborne SAR.

This thesis is made in collaboration with the Department of Signal Theory and Communications (TSC) of the Universitat Politècnica de Catalunya (UPC), which participates in the NEWA project.

Objectives

The aim of this thesis is the study and implementation of a sub-optimal space-time adaptive processing technique and its integration in the SAR processing for detection of moving targets in maritime scenario. A detection algorithm based on this technique has been implemented and its performances have been evaluated with the SAR-GMTI simulator developed in the Department of Signal Theory and Communications (TSC). The performances of this technique have been tested over different sea conditions and for different types of modeled boats.

Organization

The thesis is organized as follows:

- In chapter 1 a review of Syntectic Aperture Radar (SAR) concepts is given.

- In chapter 2 the Ground Moving Target Indicator concepts are given and the different GMTI techniques are explained.
- In chapter 3 a sub-optimal space-time adaptive processing is studied and integrated in the SAR processing for detection of moving targets and estimation of their velocity.
- In chapter 4 the simulation results of the sub-optimal space-time adaptive processing in maritime scenario are presented and commented.
- Chapter 5 summarizes the contributions of the thesis in line with some conclusions and provides general hints for future work.

Chapter 1

SAR concepts

In spaceborne SAR the Radar is mounted in a satellite, typically flying in a Low Earth Orbit. In the monostatic configuration the signals are transmitter and received by the same antenna.

Antenna pattern illuminates a specific region on the earth surface, called beam footprint, determined by the intersection of the antenna pattern and the earth surface at a given incidence angle.

As the platform advances, pulse of electromagnetic energy are transmitted at regular intervals towards the ground, this pulses, after being reflected by the ground, travel back to the Radar antenna where they are sampled according to their bandwidth.

The displacement of the satellite along its orbit provokes the displacement of the beam footprint along the earth surface, the period of time during which a point on the earth surface is illuminated by the beam footprint is called time of synthetic aperture.

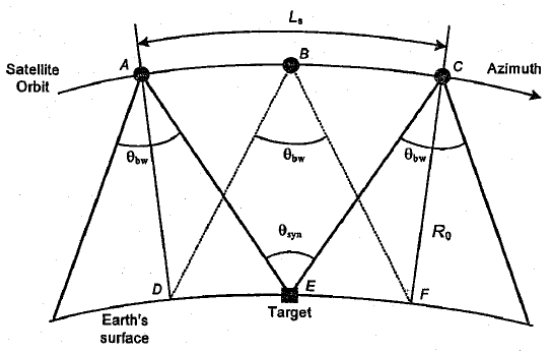

Figure 1.1: Synthetic aperture

During the time of synthetic aperture the received echoes reflected by the surface have some interesting properties that allows the coherently combination of them to synthesize an antenna length in the order of the distance covered by the radar in the time of synthetic aperture as shown in 1.1. In practice, the synthesized aperture L_s can be several thousand meters long in the spaceborne case, whereas the antenna's real aperture L_a is only on the order of 1 to 15 meters in length

The coherent combination of the echoes provides a refined azimuthal resolution

since the beamwidth is inversely proportional to the antenna aperture, independent on the range and frequency as happens in the Real aperture radars.

1.1 Spaceborne SAR geometry

The figure shown in 1.2 is useful to introduce some of the most used terms in SAR contest.

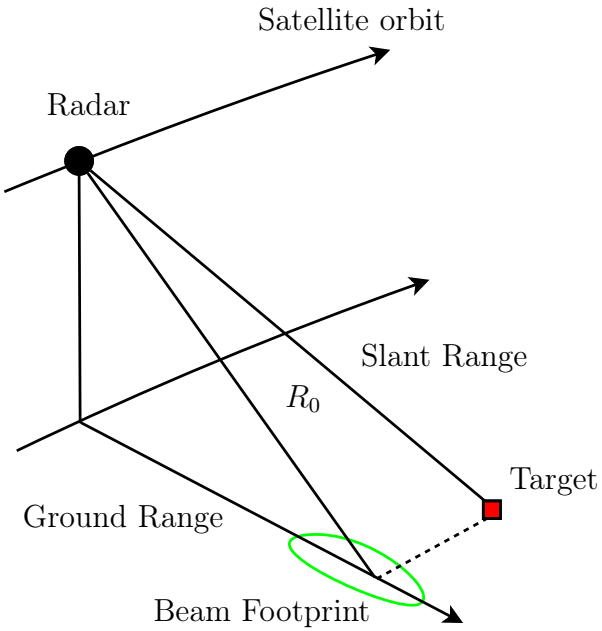

Figure 1.2: Spaceborne SAR geometry

Target: a hypothetical point on the Earth's surface that the SAR system is imaging. SAR illuminates a certain region on the earth and is able to image this region as well as the point-like scatters, which due to resolution constrains do not appear as infinitesimal point-like.

Beamwidth: the Radar beam can be viewed as a cone, and the footprint as an intersection of the cone with the ground. The beam has two significant dimensions: its angular width in azimuth and elevation planes. In both planes the beamwidth is defined by the angle subtended by the beam "edges", in which the beam edge is defined when the radiation strenght is 3dB below the maximum.

Nadir is the point on the Earth's surface directly below the sensor, so that the "normal" to the Earth's surface at the nadir passes through the sensor.

Azimuth is a direction aligned with the platform velocity, it can be considered as a vector parallel the the sensor motion

Range The slant range is measured along the radar line-of-sight while the ground range is measured along the ground. After the SAR processing, the image is

registered to the azimuth position of closest approach and the range axis is perpendicular to the azimuth axis.

Range of closest approach because of the motion of the platform the distance between the sensor and the target varies with time, when the range is a minimum it is called the range of closest approach, denoted by R_0.

Zero Doppler plane the plane containing the sensor that's perpendicular to the platform velocity vector. When this plane crosses the target, the relative radial velocity of the sensor with respect of the target is zero.

Ground range is the projection of the slant range onto the ground. Assuming that the data is registered to zero Doppler, ground range is the direction orthogonal to the azimuth axis and parallel to the earth surface with its origin at the nadir point.

Squint angle is the angle between the slant range vector and the zero Doppler plane, is an important component in the definition of the beam pointing direction.

1.2 The Range Equation

It's fundamental in the SAR processing to know how the slant range from the sensor to the target varies with time, this range history is described by the Range Equation. When the sensor approaches the target the range decreases every pulse while after the sensor passes the target the range increases every pulse. In addition to the motion of the platform also the motion of the target (if present) has to be take into account.

This change in range mainly produces two consequences:

- a phase modulation from pulse to pulse that's necessary to obtain fine azimuth resolution.
- the received data to be skewed in the computer memory, this is called range cell migration (RCM).

The following derivation of the range equation is made under the assumption of a locally straight flight path, a flat earth's surface and the absence of squint angle as shown in fig 1.3.

The azimuth direction is taken to be parallel to the motion of the sensor while range is perpendicular to it. The target and radar geometry is illustrated in fig 1.4 where the x axis represent the along-track direction, the z axis the across-track direction (on the ground) and the y axis the elevation above the Earth's surface. The Radar transmitter boarded in the satellite moves with constant velocity v_p along the azimuth axis crossing the z axis at time $t = 0$. Radar pulses are transmitted at regular intervals in time given by the pulse repetition frequency (PRF).

The point target is assumed to be at position $(0, 0, z_0)$ for $t = 0$ and it's moving with velocity components v_{x0} and v_{z0} and acceleration a_x and a_z which may be

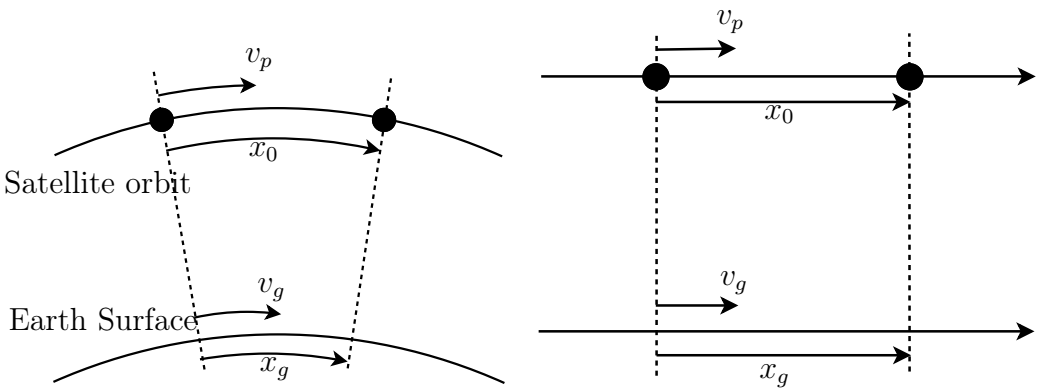

(a) *curved earth geometry.* **(b)** *flat earth geometry.*

Figure 1.3

considered constant over the observation period. The target height is assumed be zero.

We indicate with $R_0 = \sqrt{y_0^2 + H^2}$ the slant range at $t = 0$ and $R(t)$ represent the range from sensor to target at any time t. The equation that describe the temporal evolution of $R(t)$ is given by[[14]]:

$$R(t) = \left(\left(v_{x0} + \frac{a_{x0}}{2}t^2 + \frac{\dot{a_{x0}}}{6}t^3 - v_p t \right)^2 + \left(z_0 + v_{z0}t + \frac{a_{z0}}{2}t^2 + \frac{\dot{a_{y0}}}{6}t^3 \right)^2 + H^2 \right)^{\frac{1}{2}} \quad (1.1)$$

where the dots indicate time derivatives of the target acceleration. Equation 2.9 can be written as a second-order Taylor series expansion about broadside time $t = 0$ taking into account that the accelerations could be considered constants over the period of observation.

$$R(t) \approx R_0 + \frac{z_0 v_{z0}}{R_0}t + \frac{1}{2R_0}\left[(v_{x0} - v_p)^2 + v_{z0}^2 \left(1 - \frac{z_0^2}{R_0^2} \right) \right] t^2 \quad (1.2)$$

1.3 SAR Signals

1.3.1 SAR signal in Range Direction

In the range direction the radar usually sends out a pulse with a linear Frequency Modulation characteristic:

$$s_{pul}(\tau) = w_r(\tau) \cos\left(2\pi f_0 \tau + \pi K_r \tau^2 \right) \quad (1.3)$$

where K_r is the FM rate of the range pulse and $w_r(\tau)$ denotes the pulse envelop that used to be approximately rectangular as expressed in equation 1.4 where T_r is the pulse duration.

$$w_r = rect\left(\frac{\tau}{T_r} \right) \quad (1.4)$$

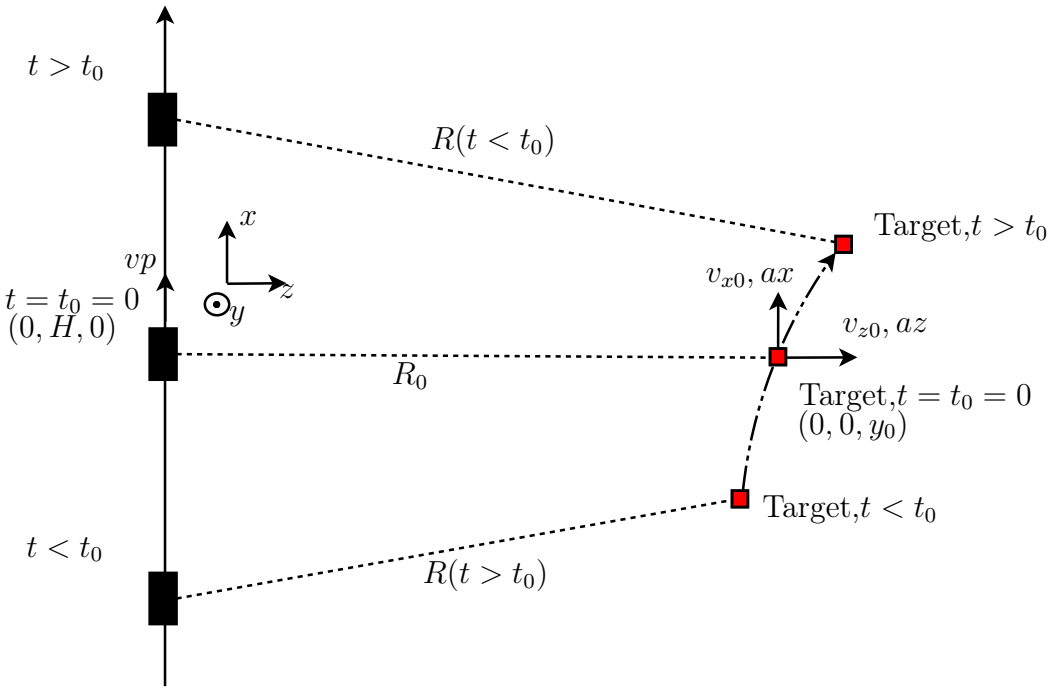

Figure 1.4: Top-down view of antenna and accelerating target geometry for a space-borne scenario

From now on we'll refer to the time τ as the fast time because the range signal travels at the speed of light while the azimuth signal is originated by the movement of the platform.

The instantaneous frequency of the signal $s_{pul}(\tau)$ varies with the fast time τ, in fact if we take the derivative of the argument of the cosine we find that the instantaneous frequency $f_i = f_0 + K_r\tau$.

When the sign of K_r is positive then the signal is called an up-chirp while in the other case corresponds to a down-chirp. This characteristic of the signal neither affects the structure of the SAR processing nor the quality of the processed image.

One very important parameter is the bandwidth of the signal, since the resolution of the SAR image and the sampling requirements are directly dependent on it. The bandwidth of the signal $s_{pul}(\tau)$ is given by $BW = \|K_r\|T_r$.

The demodulated signal is digitized at a sampling frequency F_r above the Nyquist criterion. In practice the sampling frequency is chosen to oversample the signal by a factor that is called range oversampling ratio $\alpha_{os,r}$ and is usually between 1.1 and 1.2.

Let's now analyze the received signal. The Radar beam has a certain beamwidth in the elevation plane, illuminating a section of the ground, lying between the "near range" and "far range" as indicated in figure 1.5.

The transmitted pulse travels at the speed of light towards the earth surface, at time t_1 the pulse reaches the ground at the "near range" and after a fraction of millisecond the trailing edge of the pulse passes the "far range" point at time t_2.

The reflected energy at any illumination instant is a convolution of the pulse waveform and the ground reflectivity within the illuminated patch.

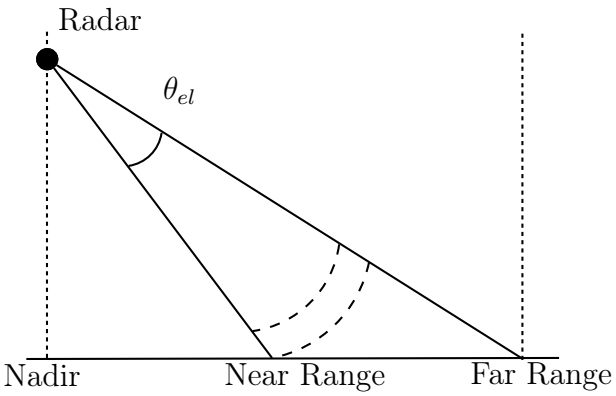

Figure 1.5: Radar beam's $3dB$ elevation beamwidth

$$s_r(\tau) = g_r(\tau) \otimes s_{pul}(\tau) \tag{1.5}$$

This energy arrives back at the receiving antenna between times $2t_1$ and $2t_2$, the receiver starts sampling a few milliseconds before $2t_1$ and ends a few milliseconds after $2t_2$.

The distance between the near-range and far-range is called swath width, and cannot be chosen arbitrarily.

It's very important for the elevation beam to be not too wide in relation to the interpulse period because in this case range ambiguities may occur which result from the mixing of reflected energy from consecutive pulses at the receiver.

1.3.2 SAR signal in Azimuth Direction

As the platform advances along its path, subsequent pulses are transmitted and received by the radar. These pulses are transmitted every $PRI = \frac{1}{PRF}$ where PRF is defined as pulse repetition frequency.

SAR doppler frequency

During the data acquisition the signal is transmitted through the antenna, and the resulting electromagnetic wave travels to the ground where it hits an object and is reflected. The reflected wave travels back to the antenna and has the same waveform as the transmitted signal but is much weaker and has a frequency shift due to the relative speed of the sensor and the object.

A given point in the ground passes through the whole antenna main beam as the platform moves, varying its slant range. It is precisely this range variation, which induces a parabolic phase variation producing a frequency modulation in the azimuth dimension similar to the transmitted chirp pulse.

The Doppler bandwidth is defined by the antenna mainlobe.

Pulse transmission and receiving

The transmitted pulses are equally spaced and are coherently transmitted, that means that the start time and phase of each pulse is carefully controlled.

In the receiver chain the demodulator must maintain high time accuracy as well. This coherency is an important property, necessary to obtain high azimuth resolution in SAR system.

During the echo window (radar not transmitting) the radar acquires the reflected echoes. It's a common rule to put some guards times between the transmission windows and the receiving one to allow the system to switch and to prevent unwanted superpositions between transmitted and received pulse.

Choice of PRF

The most important parameters to be taken into account when choosing a PRF are the followings:

Nyquist sampling rate The PRF should be larger than the significant azimuth signal bandwidth. The azimuth oversampling factor $\alpha_{os,a}$ is usually about 1.1 to 1.4. If the PRF is too low than azimuth ambiguities caused by aliasing will be troublesome.

Range swath width The sampling window con be up to $\frac{1}{PRF} - T_r$ seconds long, corresponding to a slant range interval of $\left(\frac{1}{PRF} - T_r\right)\frac{c}{2}$ meters. The PRF should be low enough so that most of all the near to far range interval illuminated by the beam falls within the receiver window. If the PRF is too large in relation to the echo duration, range ambiguities occur because of echoes from different pulses overlapping in the receive window.

Receive window timing The significant energy from the ground must arrive at the receiving antenna between the pulse times,, this concerns the start time of the window. The start time is particulary affect by the PRF in the spaceborne case when a given transmitted pulse is not received until several pulse intervals are elapsed.

Each of these criteria is in conflict with some of all of the other criteria, so a compromise is needed, especially in the spaceborne case. The tradeoff involves many of the SAR system parameters like platform height and velocity, operating range, radar wavelength, antenna length and range swath width.

Azimuth signal strength and doppler history

As the platform moves a target on the ground is illuminated by hundreds of pulses. While the strength of the transmitted pulse is constant, the strength of the echoes is not constant because of two main causes:

- The azimuth beam pattern.
- The variation of the sensor-target distance.

the first one is certainly the most effective. To explain this effects figure 1.6 can be of help, in which an azimuth beam pattern for a zero squint angle is shown. As

the sensor moves along its path the angle between the sensor path and the sensor-target direction changes. The received signal strength is shown in the middle part of the figure, it increases until the target lies in the center of the beam and after the beam center crossing time it decreases until the target lies in the first null of the beam pattern.

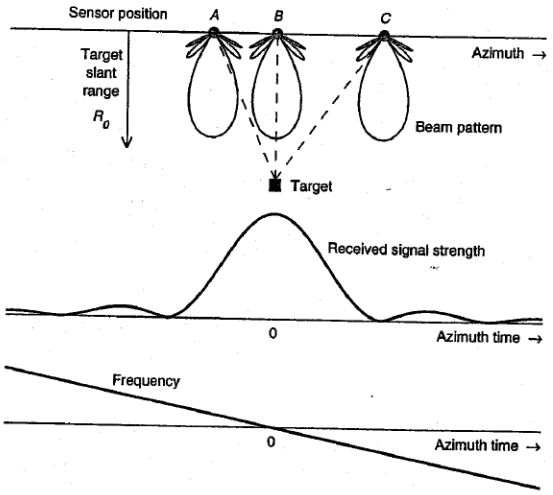

Figure 1.6: Azimuth beam pattern and its effect upon signal strength and doppler frequency, extracted from [9]

The energy in the outer edges of the main lobe, as well as the energy in the sidelobes, contribute to the azimuth ambiguities in the processed image. In the bottom part of the figure the doppler frequency history of the target is shown, it is proportional to the target's radial velocity with respect to the sensor.

Doppler Bandwidth

Considering the platform velocity v_p, the $3dB$ azimuth beamwidth of the radar beam θ_{bw}, the central wavelength of the radar λ and assuming a zero squint angle case, the doppler bandwidth is given by:

$$\Delta f_{dop} = \frac{2v_p}{\lambda}\theta_{bw} \tag{1.6}$$

This bandwidth governs the sampling requirements.

Azimuth FM rate

The azimuth FM rate is the rate of change of azimuth or doppler frequency. It can be calculated taking into account the range equation as it gives the phase history of the azimuth signal. Considering a second order Taylor approximation of the target's phase history (under static conditions), the received signal has a quadratic phase term like in the range signal so it's a chirp signal with a linear frequency variation in time. The FM rate K_a can expressed as:

$$K_a = -\frac{\Delta f_{dop}}{T_a} = -\frac{2v_p^2}{\lambda R_0} \tag{1.7}$$

where the minus sign comes from the fact that the change of the doppler frequency has a negative trend as shown in fig 1.6.

1.4 SAR resolution

The term resolution in radar contest is the capability of the radar to distinguish two targets that differ in their position on the ground. In SAR, fine azimuth and range resolution is obtain applying a matched filter, there's a lot of literature on this subject and on pulse compression techniques of linear FM signals, here only the main results are reported.

1.4.1 Range resolution

In the range direction, the received signal has FM characteristics, inherited from the transmitted pulse. High range resolution is obtained matched filtering the return signal with a reference transmitted chirp pulse. The resolution is inversely proportional to the pulse bandwidth:

$$\Delta R = \frac{c}{2B} \tag{1.8}$$

where c is the speed of light and B is the bandwidth of the transmitted signal.

1.4.2 Azimuth resolution

In the azimuth direction if we assume that the beamwidth is $\theta_{bw} \approx \frac{0.886\lambda}{L_a}$ (that's an approximation based on a sinc-shape azimuth beam pattern) where L_a is the antenna length, the azimuth resolution of the real aperture is given by the projection of the beamwidth onto the ground:

$$\Delta Az_{uncomp} = R_0\theta_{bw} = \frac{0.886\lambda R_0}{L_a} \tag{1.9}$$

that could be of the order of several kilometers in the spaceborne case. An improved resolution is achieved by means of the formation of the synthetic aperture (coherent integration of the pulses), such that the frequency modulated signal in the azimuth dimension can be compressed using a matched filter approach (as in the range dimension).

$$\Delta Az \approx v_p \frac{0.886}{\Delta f_{dop}} \approx \frac{L_a}{2} \tag{1.10}$$

The result is that the azimuth resolution is approximately half the antenna length independently of range, velocity and wavelength.

Chapter 2

SAR GMTI concepts

SAR systems provide bidimensional radar images of earth surface and they were not originally devoted to extract information of moving targets. GMTI has the aim to detect moving targets, which may compete against what is called clutter that is the static background scene in this case.

Before introducing the GMTI techniques is it necessary to understand the spectral characteristics of a moving target echo and the differences respect to a static object or clutter, which can be precisely exploited to detect and estimate the different parameters of the moving targets.

2.1 Moving Targets

A moving single point target has a phase history different from a static point in the scene; this difference due to its velocity and acceleration components appears clear in the range equation:

$$R(t) \approx R_0 + \frac{z_0 v_{z0}}{R_0} t + \frac{1}{2R_0}\left[(v_{x0} - v_p)^2 + v_{z0}^2\left(1 - \frac{z_0^2}{R_0^2}\right)\right] t^2 \tag{2.1}$$

This difference can be analyzed in the time or in the frequency domain, both of them can be exploited by the detection and estimation techniques.

2.1.1 Across-track velocity

A non zero across-track velocity v_{z0} add the term $\frac{z_0 v_{z0}}{R_0} t$ in the range equation equation 2.1. The moving target signal $s(t)$, neglecting the accelerations can be expressed as:

$$s(t) = Aexp(-j2\beta R(t)) \approx Aexp(-j2\beta(R_0 - \frac{v_p}{2R_0} t^2))exp(-j2\beta \frac{z_0 v_{z0}}{R_0} t) \tag{2.2}$$

where $\beta = \frac{2\pi}{\lambda}$ is the wavenumber and A the amplitude of the pulse reflected by the target. The first term of the signal $s(t)$ has the same phase history of a static target, whereas the second one due to the across-track velocity v_{z0} add a linear phase term that changes the instant frequency of the received signal (Doppler

effect). This linear phase term, in frequency, provokes the shift of the spectrum of a static target. The bandwidth of the signal in the azimuth direction remains unchanged, but the spectrum is shifted in frequency according to the doppler offset:

$$\Delta f = 2\frac{v_z}{\lambda}\sin\theta_{inc} \tag{2.3}$$

where v_z is the along-track velocity of the target, λ the Radar wavelength and θ_{inc} is the incidence angle between the beam and the earth surface.

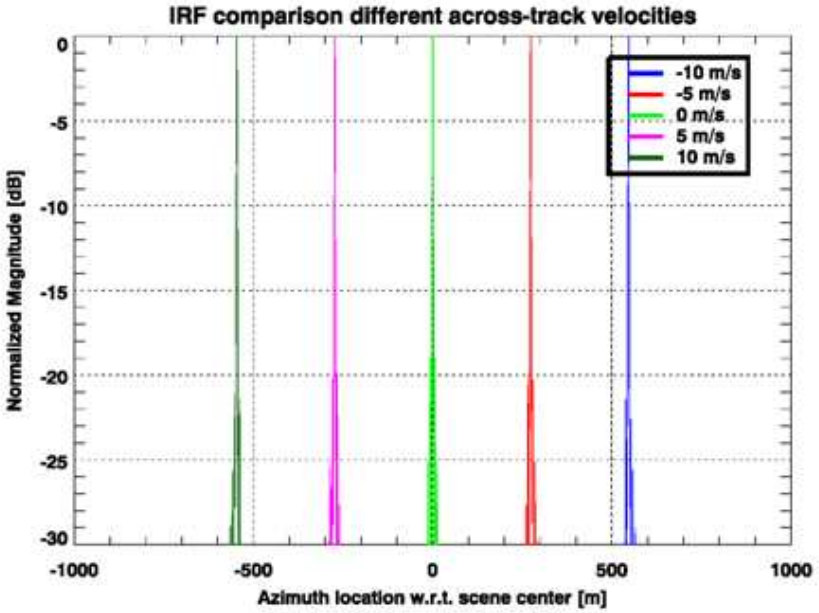

Figure 2.1: Azimuth cut of the impulse response function of a moving target with different constant across-track velocities

If compressed with a Static Word Matched Filter (which focuses all the targets to their zero-Doppler position) the image of a moving target with along-track velocity has azimuthal displacement as shown in fig 2.1.

2.1.2 Along-track velocity

A constant across-track velocity v_{x0} change the quadratic phase term of the moving target signal respect to a static one, as can be noted in:

$$R(t) \approx R_0 + \frac{1}{2R_0}\left[(v_{x0} - v_p)^2\right]t^2 \tag{2.4}$$

where again v_p is the along track velocity. In the azimuth dimension the signal is a chirp-like function but with a different rate due to the change in the relative motion between the target and the platform $(v_{x0} - v_p)$. The Doppler bandwidth of the signal in the azimuth direction changes depending on the magnitude and direction of the along-track velocity.

- if the along-track velocity v_x and the platform velocity v_p have the same sign, the relative platform-target velocity decrease and so does the doppler slope. The bandwidth of the signal decreases.

- if v_x and v_p have opposite sign, than the relative platform-target velocity increases and so does the doppler slope. The bandwidth of the signal increases.

Should be noted that in spaceborne SAR the platform velocity v_p could reach several $\frac{Km}{s}$ whereas the target velocity v_x is in the order of tens $\frac{m}{s}$ so the bandwidth variation are not so big. If compressed with a SWMF the image of a moving target with only along-track velocity has azimuthal defocusing and amplitude reduction as can be seen in figure 2.2.

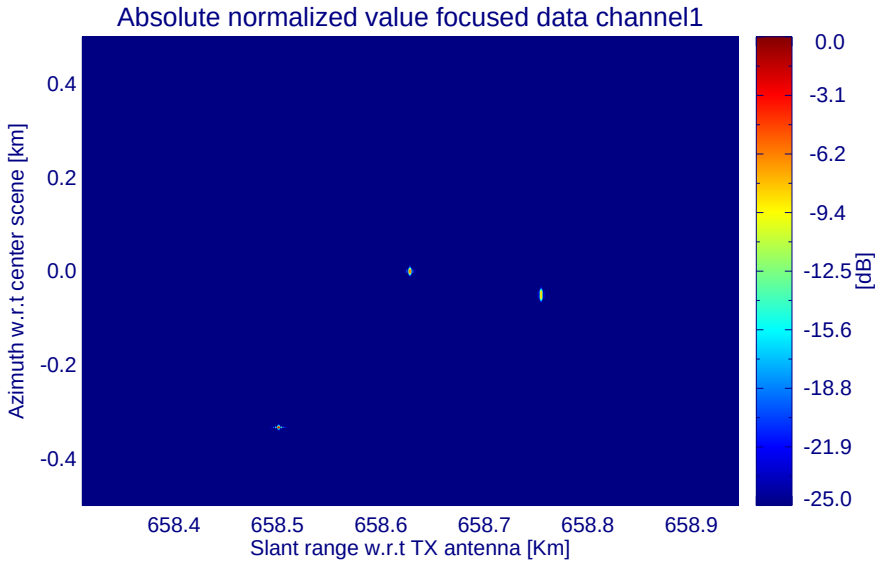

Figure 2.2: Focused SAR image of three moving target with, from the left,$v_x = 0\frac{m}{s}, v_x = 10\frac{m}{s}, v_x = 20\frac{m}{s}$

2.2 Clutter

The word clutter is used to describe that part of the observed scene that is not of interest for GMTI. It can be viewed as the sum of all the echoes from the non moving scatters. It is not easy to describe the clutter characteristics because they depend on different parameters[10] as:

- type of surface (land, sea, urban area).
- incidence angle.
- polarization.
- decorrelation processes.
- wavelength.

The clutter is commonly characterize by its backscattering coefficient $\sigma 0$ (measured in $\frac{dBsm}{sm}$) and its statistical properties. If we assume that the clutter distribution is spatially stationary, i.e. that the statistical properties are invariant with azimuthal shifts, the clutter distribution is characterized by the covariance function:

$$R_z(\tau) = E[p(t)p^*(t+\tau)] \tag{2.5}$$

where E denotes the expectation operator and $p(t)$ is the clutter azimuthal reflectivity. This function depends on the spatial behavior of the clutter: it reflects its smoothness or rapid changes in the reflectivity. In most cases, but not always, it will be appropriate to assume spatially white clutter, especially if many scatterers independent and identically distributed (from the central limit theorem) are contained in each resolution cell.

2.3 Multichannel SAR

Different procedures have been proposed to detect moving targets with single channel SAR systems. In one of them the moving targets are detected because their frequencies fall outside the main-beam clutter band.

The effectiveness of these procedures are quite limited becasuse the slowly moving targets are completly masked by the clutter Doppler spectrum. Even in the case of highly moving targets part of their doppler frequencies fall into the clutter band because in SAR system the PRF is limited as we have seen in chapter 1. Consequently is not possible to perform a good clutter cancelation by filtering in frequency domain.

This problems can be overcome using a multichannel SAR.

2.3.1 Dual Receive Antenna

The current implementation of SAR missions (Terrasar-X, Radarsat-2 and the future Spanish PAZ) are not specifically designed for the GMTI, they have instead some experimental GMTI modes of operation.

These missions have two physical receiver chains, therefore the maximum number of channels that can be simultaneously recorded is set to two. These missions are equipped with a highly flexible phased array antennas.

In the Dual Receive Antenna mode of operation the complete antenna is used for transmission but in receive the antenna is divided into two halves in along-track. The signals of both receiving antennas are sampled and recorded separately.

A direct consequence of this partitioning is that the azimuth pattern of the two halved partitions are doubled in beamwidth compared to the complete antenna, this clearly impacts on the doppler bandwidth and indeed on the PRF choice. It has also to be kept in mind that the Rx gain is reduced by $3dB$ for a halved receive antenna.

Anyway this impact is not so important because the two-way pattern has to be considered for each channel where the smaller beamwidth of the transmission antenna mitigate the broadening effects of the receiving one.

This new spatial degree-of-freedom (DoF) provided by the second channel could be spent to suppress clutter or to perform a better estimation of the target parameters, but the total number of DoF provided by the DRA are not enough to simultaneously suppress the clutter and accurately estimate the target's parameters, such as velocity and location.

2.3.2 Toggle Modes

Current platforms (or near future ones) are limited to two physical receiving chains for cost and practical reasons. The idea proposed by S.Chiu in[**Chiu**] is that by doubling the pulse repetition frequency (PRF) of the radar it is possible to generate one or two additional channels.

In the toggles modes , the flexibility on the array antenna's programming, is exploited to generate additional virtual channels (three or four in the considered cases) at different pulses.

In all the considered toggle modes the period of cyclical programming of the TX/RX schemes of the antenna is set to two. In order to avoid eventual clutter band aliasing the PRF have to be doubled.

2.3.3 Toggle receive modes

In the toggle receive modes the pulses are transmitted exploiting the full antenna aperture and the echoes are received using two alternating receiver excitation schemes.

Three virtual channel toggle on receive mode In figure 2.3 is shown a possible way to implement a three virtual channels channel toggle on receive scheme: during odd pulses the transmission is done with the whole antenna and the backscattered signal is received with the two sub-apertures obtained splitting up the whole antenna in two equal parts; in the second pulse the signal is transmitted with the whole antenna and the backscattered signal is received with a single centered sub-aperture.

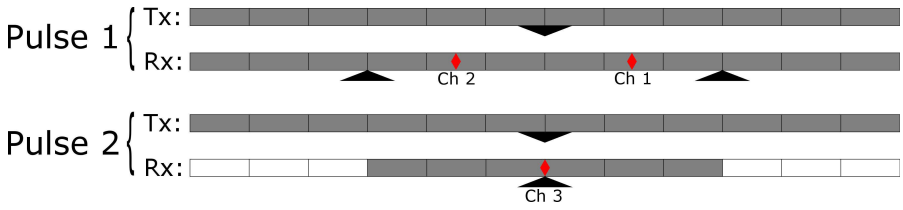

Figure 2.3: Three virtual channel toggle on receive configuration of the antenna for the different pulses, the black triangles indicates the physical centers of the Tx or Rx antennas, the red diamonds indicates the two-way phase centers for each virtual channel

Some considerations have to be done for this mode of operation, in fact in order to avoid aliasing problems the PRF has been doubled and this implies that to keep a power consumption similar to the DRA mode the energy-per-pulse have to be

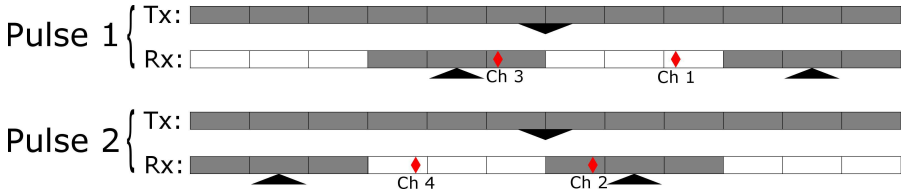

Figure 2.4: Four virtual channel toggle on receive configuration of the antenna for the different pulses, the black triangles indicates the physical centers of the Tx or Rx antennas, the red diamonds indicates the two-way phase centers for each virtual channel

reduced by the same amount the PRF is increased. The Signal to Clutter Ratio (SCR) doesn't change because the energy of the clutter is dependent by the energy of the pulse, but the Signal to Noise Ratio (SNR) decrease.

Four virtual channels toggle receive mode In figure 2.4 is shown a possible way to implement a four virtual channel toggle on receive scheme: during the odd pulses the transmission is done with the whole antenna and the backscattered signal is received with two sub-apertures obtained splitting up the whole antenna in four equal parts and activating only two of them, in the even pulses the signal is transmitted with the whole antenna and the backscattered signal is received with two remaining sub-apertures.

In this mode of operation the SNR decrease even more respect the previous mode because of the reduced length of the receiving sub-apertures(the RX antenna is a quarter of the TX).

2.3.4 Toggle on transmit modes

In the toggle on transmit mode the pulses are transmitted exploiting half of the antenna aperture, such that the transmission is cyclical (on the pulse basis) alternate from fore to aft parts. The echoes are received using two sub-apertures of the full antenna (as in the Double Receive Antenna mode).

Three virtual channels toggle on transmit mode In figure 2.5 is shown a possible way to impleent a three virtual channels toggle on transmit scheme: during odd pulses the transmission is done with half of the whole antenna (fore part) and the backscattered signal is received with two sub-apertures; in the even pulses the signal is transmitted with the aft part of the whole antenna and the backscattered signal is received with the same two sub-apertures as for odd pulses.

should clarify that is four times higher due to the cyclical approach (x2) and due to the broader two-way pattern (x2)

In order to avoid aliasing problems in this mode, the PRF should be quadrupled because, in fact as in the other modes the cyclical approach need a doubled PRF, but here also the broader two-way pattern caused by the transmission with one partitioned antenna needs to be taken into account because it increases the Doppler band of the azimuth signal so that a quadrupled PRF is needed to avoid aliasing.

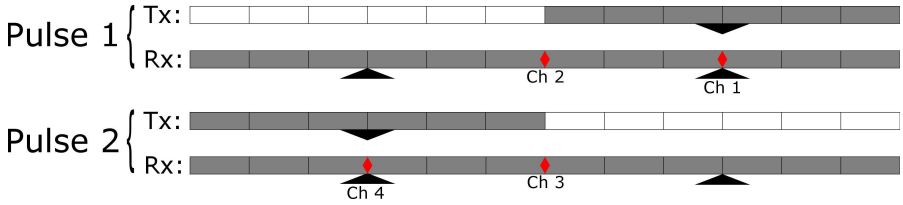

Figure 2.5: Three virtual channels toggle on transmit mode configuration of the antenna for the different pulses, the black triangles indicates the physical centers of the Tx or Rx antennas, the red diamonds indicates the two-way phase centers for each virtual channel

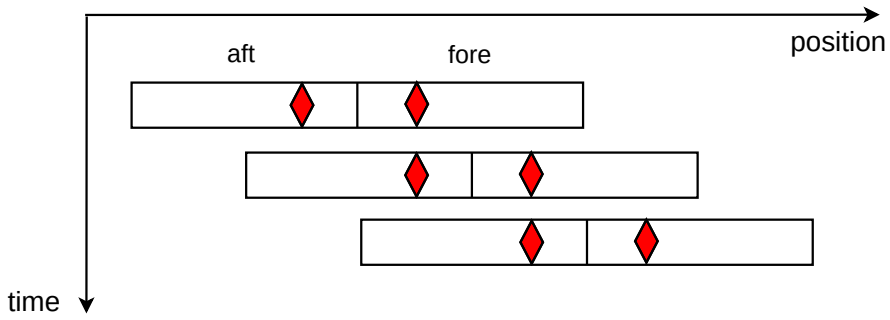

Figure 2.6: DPCA principles, red diamonds indicates the 2-way phase center of the aft and fore antenna

This is a very hard request for the actual spaceborne SAR systems where the flexibility in the choice of the PRF has not this dynamic range (the PSEORAR/-PAZ for example has a nominal PFR of $3.92kHz$ that can be increased to a maximum of $7kHz$).

2.4 GMTI Techniques

2.4.1 Displaced Phase Center Antenna

The working principle of DPCA is showed in fig 2.6 :the radar antenna is moving along track when the two pulses are transmitted and corresponding echoes received. If PRF is adjusted to the RX separations and satellite velocity in a way that the aft antenna occupies, at the second (even) pulse, the same position as the fore for the first (odd) pulse, the clutter is seen at two different time instants from the same radar location: the platform motion has been compensated, consequently the Doppler spectrum of clutter is not spread due to platform motion.

The clutter is cancelled by subtracting the echoes of the first pulse received by the fore subarray from the echo of the second pulse received by the aft subarray.

Stationary targets should cancel, moving targets with a radial velocity component will arise a phase shift, so the output of the two pulse canceller will not vanish making the detection possible.

The PRF-velocity constraint to satisfy the DPCA condition can be relaxed by digitally re-sampling (interpolating) the data in order to adjust digitally the DPCA condition.

The sensitivity of DPCA depends on the distance between the two antennas (considering the two-way pattern) that is called base-line, a longer base-line provides higher sensitivity but at the same time leads to a comb of blind velocities (when the phase difference of the tho channels is an integer multiple of 2π)

2.4.2 Along Track Interferometry

In the Along-Track Interferometry, similar to the DPCA technique, two displaced antennas along-track are used. For each of the two channels a SAR image is generated, and in the azimuth compression the time delay between the two channels is compensated (the two images are spatially co-registrated). Then if the first image is multiplied by the complex conjugate of the second, the remaining phase is zero for non moving target and different from zero, otherwise.

If the two receiving antennas are separated in azimuth by a distance d, then the interferometric phase is approximately given by:

$$\Delta\Phi = -\frac{2\pi}{\lambda} d \frac{v_r}{v_p} \tag{2.6}$$

where v_r is the radial velocity of the target that is related to the across-track velocity $v_r = v_{across-track} \sin\theta_{inc}$ and θ_{inc} is the incident angle of the beam on the earth surface.

One shortcoming of ATI is that to get a high sensitivity, the two antennas have to be separated far away and this is not a trivial task in a spaceborne platform. Having a large antenna separation on the other hand leads to a comb of blind velocities (when the phase difference of the tho channels is an integer multiple of 2π):

$$v_{blind} = k v_p \frac{\lambda}{d} \tag{2.7}$$

where v_p is the platform velocity and k is integer. These blind velocities thin out the interesting velocity range.

2.4.3 STAP

Space Time Adaptive Processing is the natural generalization of DPCA, in fact it has the following features:

- generalization of DPCA for clutter cancellation.
- generalization of adaptive array of antennas for jammer nulling (mostly used in military applications).
- freedom in shaping the null.
- fewer constraints on the spacing of the antenna elements.
- compensation of platform motion along (as DPCA) and orthogonal to the array thus avoiding clutter spectral spreading.

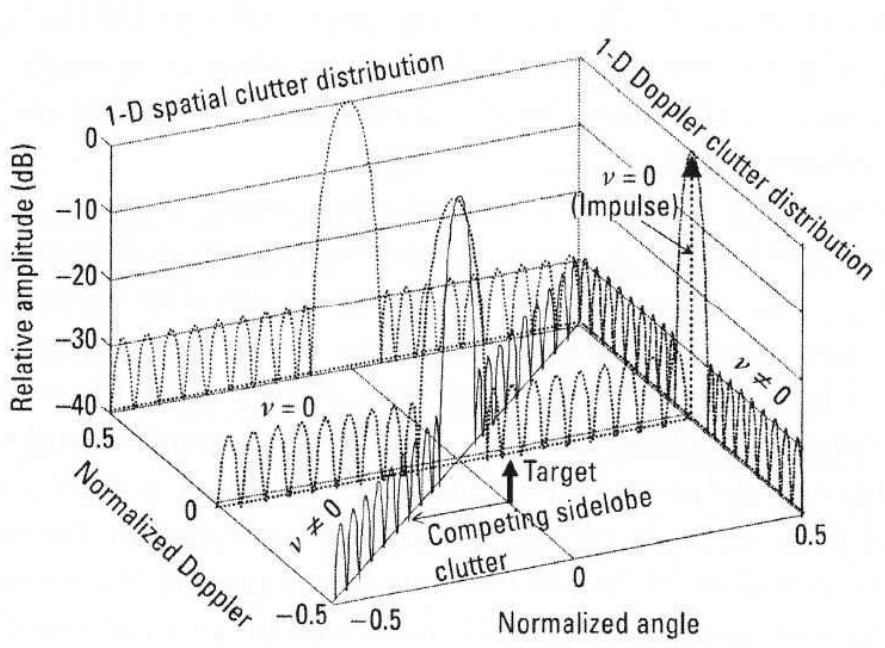

Figure 2.7: power spectral density of the clutter in the angle-Doppler domain (ridge-like pattern of the clutter due to motion of the platform); extracted from [8]

The need for joint space and time processing arise from the inherent two-dimensional nature of ground clutter. In figure 2.7 the distribution of ground clutter (power spectral density arising from the two-way antenna pattern) for a side-looking radar with a uniform linear array is illustrated as a function of normalized angle (the spatial dimension) and normalized Doppler (the temporal dimension). Because of the platform motion the ground returns are doppler shifted according to the relationship

$$f_d = \beta\theta \tag{2.8}$$

where θ and f_d are the normalized angle and Doppler respectively and β is a proportionality constant that depends on ownship speed, PRF, and antenna separation.

In addition to this, due to the sampling of the azimuth signal at PRF, there could be a clutter region with the same Doppler frequency, but at different position (an angle offset) because of the aliasing.

The objective of the space-time processing is to place a null in the angle-Doppler beampattern where clutter may compete.

Apparently from this introduction the adaptivity is not needed since it is conceivable to know the relative orientation of the radar and ground surface as well as basic ground topology. Knowing this one could simply steer a deterministic null in the predicted clutter direction.

Unfortunately there're a lot of practical real-world considerations that severely limits the efficiency of this technique such as:

- channel mismatch

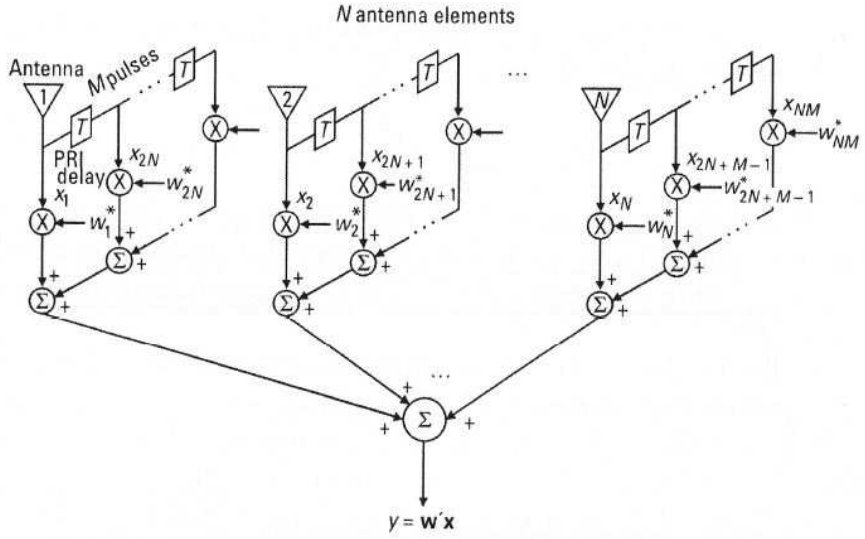

Figure 2.8: STAP beamformer, extracted from [8]

- clutter heterogenity/nonstationarity

This real-world consideration give rise to the inherent need for adaptivity.

In figure 2.8 the basic schematic architecture of a STAP beamformer is shown, in which an M coherent pulses interval of an N elements antenna array is processed.

As with an ordinary one-dimensional spatial-only beamforming, a two-dimensional angle-Doppler (space-time) beampattern can be formed by a judicious selection of a complex linear combiner weights w_i.

Has been demonstrated that to maximize the response to a uniform narrowband plane-wave corresponding to a given angle and Doppler the linear combiner weight vector $\mathbf{w}$ should be set equal to the anticipated structure of the desired signal $\mathbf{s}$.

The result of this will be a two dimensional pattern (angle-Doppler) that has the peak in correspondence to the target (signal) of interest.

A linear combiner of this type has NM degrees of freedom, this means that for a desired angle-Doppler look direction $\mathbf{s}$, we could also specify up to $NM - 1$ "nulls".

If the set of NM angle-Doppler vectors $\mathbf{s}, \mathbf{j_1}, ..., \mathbf{j_{NM-1}}$ is linearly indipendent then a deterministic set of beamformer weights can be obtained from a linear set of equations:

$$\begin{bmatrix} \mathbf{w's} = 1 \\ \mathbf{w'j_1} = 0 \\ \dots \\ \mathbf{w'j_{NM-1}} = 0 \end{bmatrix} \tag{2.9}$$

Unfortunately, due to the relative strength of potential interference (clutter and/or jamming) and the practical limitations on deterministic nulling, this approach is unsustainable in practice.

Radar community has looked towards statistical signal processing for a means of addressing the limitations of deterministic nulling. In particular clutter and jam-

ming are treated as stochastic processes and the optimum space-time beamformer is derived via a statistical optimization procedure. Although there are many variations on the theme, the basic underlying beamformer results is given by:

$$\mathbf{w} = \mathbf{R^{-1}s} \tag{2.10}$$

where $\mathbf{R}$ is the positive-definite $NM * NM$ dimensional covariance matrix associated with the total interference (clutter, jamming, receiver noise).

It is possible to estimate $\mathbf{R}$ from sample data obtained in the normal course of radar operation, it is this estimation of $\mathbf{R}$ on the fly that is the true basis for the inclusion of the word "adaptive" in STAP.

Chapter 3

Detection and Estimation Algorithm

The objective of this thesis is to implement and evaluate the performance of a STAP processing scheme on a multichannel spaceborne GMTI SAR. This evaluation is based based on simulated SAR data for the future Spanish SEOSAR/PAZ mission.

3.1 Post Doppler STAP

In spaceborne SAR the length of the synthetic aperture could be in the order of several Km, and the number of azimuth samples that can be processed coherently M is indeed in the order of thousand.

A fully optimum STAP implementation would require the solution of a $NM \times NM$ problem, where M is the number of pulses considered for the processing and N is the number of channels. The solution of such problem is not simple and have a very high computational cost due to the inversion of the clutter plus noise covariance matrix thas has dimensions $NMxNM$.

One efficient implementation suitable for SAR is Post-Doppler STAP in which clutter cancellation is performed in the Doppler domain for each Doppler component using just the spatial degrees of freedom. The original $NM \times NM$ dimensional problem is split into M separates $N \times N$ independent problems.

For a sufficiently long time base of the Fourier transform (in the case of spaceborne SAR the length of the synthetic aperture), the frequency bins in the Doppler domain can be considered mutually independent [10].

The optimum spatial-only beamformer for each frequency ω is then given by:

$$\mathbf{w}(\omega) = \mathbf{R}^{-1}(\omega)\mathbf{u}(\omega, \xi) \tag{3.1}$$

where $\mathbf{a}(\omega, \xi)$ is the expected steering vector $(1 \times N)$ for the target on interest with parameters $\xi = [v_{along}, v_{across}, x_0]$ that the STAP should maximize and $\mathbf{R}$ is the $N \times N$ spectral power density matrix of clutter plus noise.

The model of the received signal from a target for a given channel i in time is given by:

$$s_i(t, \xi) = D_i(u_i(t, \xi))e^{j2\beta R_i(t,\xi)} \tag{3.2}$$

where $R_i(t,\xi)$ is the slant range distance, $\beta = \frac{2\pi}{\lambda}$ is the wavenumber and $u_i(t,\xi)$ the direction history (directional cosine) from the i-th antenna to the moving target on the ground. $D_i(u(t,\xi))$ describes the two-way antenna pattern of the $i-th$ channel. In the far-field assumption, $u_i(t,\xi) = u(t,\xi)$, the distances can be rewritten as $R_i(t,\xi) = R(t,\xi) + u(t,\xi)d$, where d is the spacing between the receivers and $R(t,\xi)$ the slant range distance from any reference channel to the target. For the particular case of a dual-receive channel the two dimensional signal vector becomes:

$$s(t,\xi) = e^{j2\beta R(t,\xi)} \begin{bmatrix} D_1(u(t,\xi)) \\ D_2(u(t,\xi))e^{j\beta u(t,\xi)d} \end{bmatrix} = e^{j2\beta R(t,\xi)}\mathbf{a}(u(t,\xi)) \tag{3.3}$$

In array processing terminology the vector $\mathbf{a}(u)$ is called the steering vector. In post-Doppler STAP we process the signal in the Doppler domain so we are interested in the fourier transform of (3.3) that can be written in analytical form as:

$$\mathbf{S}(\omega,\xi) = \gamma(\omega)\mathbf{a}(u(\omega,\xi)) \tag{3.4}$$

which can be expressed as the multiplication of the steering vector $\mathbf{a}(u(\omega,\xi))$ by the fourier transform of the phase history signal of the target $\gamma(\omega)$.

The directional cosine $u(\omega,\xi)$ can be calculated as:

$$\begin{aligned} u(\omega,\xi) = &- \frac{(v_{along} - v_p)\omega}{2\beta[(v_{along} - v_p)^2 + v_{across}^2]} \\ &+ \frac{v_{across}}{\sqrt{(v_{along} - v_p)^2 + v_{across}^2}}\sqrt{1 - \frac{\omega}{2\beta\sqrt{(v_{along} - v_p)^2 + v_{across}^2}}} \end{aligned} \tag{3.5}$$

The multiplication by the conjugate transpose of the steering vector in 3.7 maximize the beamformer response for a given target with a directional cosine history $u(t,\xi)$.

The spectral power density matrix $\mathbf{R}$ of clutter plus noise can be estimated from a training data. For each Doppler frequency ω all the range bins can be used in the estimation and hence the estimation possesses a very low variance:

$$\mathbf{R}(\omega) = \frac{1}{k}\sum_{r=R_{min}}^{R_{max}} \mathbf{x}(r,\omega)\mathbf{x}^*(r,\omega) \tag{3.6}$$

where $\mathbf{X}(r,\omega)$ is the vector of the received signal and k is the number of training vectors used for the estimation.

For a good estimation of $\mathbf{R}$ matrix, the training data over which the estimation is done should contain only clutter and noise, in the simulation the $\mathbf{R}$ matrix is estimated over a training data which contain only clutter and noise.

The process to invert this matrix is called the SMI (Sample Matrix Inversion) and the number of k training vectors to be used is higher than $2NM$ for the general case in order to obtain a degradation of the performance below $3dB$ compared to ideal case of exactly knowledge of the matrix [see REF: Melvin: "A STAP overview"]

Under this premise, the Signal Clutter Noise Ratio (SCNR) optimum filter for a particular frequency ω is given by:

$$y(\omega) = \mathbf{w}^h(\omega) * \mathbf{x}(\omega) \tag{3.7}$$

where H is the transpose conjugate operator.

The STAP filtering provides the clutter cancellation and the maximization of the signal of a particular target of interest but doesn't compensates for the phase history of the target.

This last step required to concentrate the energy of a target signal is the azimuth compression that is usually done in the range-Doppler domain by the multiplication for the complex conjugate of $\gamma(\omega)$. Generally there's no a-priori information on the target characteristics hence in the compression the phase history of a static target is used (SWMF).

3.2 Detection

The algorithm for the detection is schematically depicted in 3.1 :

- The raw data file of the M channels is organized in a cube matrix. In a first step a Range-Compression is performed for each channel.
- At the range-compressed data the Range Cell Migration Correction (RCMC) is applied for each channel.Its an important step in order to focus the different targets with the expected azimuth resolution, such that the energy spread over azimuth is concentrated over the same range line.
- After RCMC, a FFT in azimuth dimension is applied such that the clutter cancellation is performed in the Range-Doppler domain.
- For each doppler frequency the matrix $\mathbf{R}(\omega)$ is estimated using the different range bins (for this spectral component)in the training data that contains only clutter and noise.
- Afterwards, the post-Doppler STAP processing is performed for each range-Doppler bin.
- A SWMF azimuth compression performed in the Doppler domain
- An azimunt IFFT applied to return to obtain a SAR image, where the clutter has been cancelled out.
- The magnitude of every single bin of the image is compared to a threshold and a Detection image is produced.

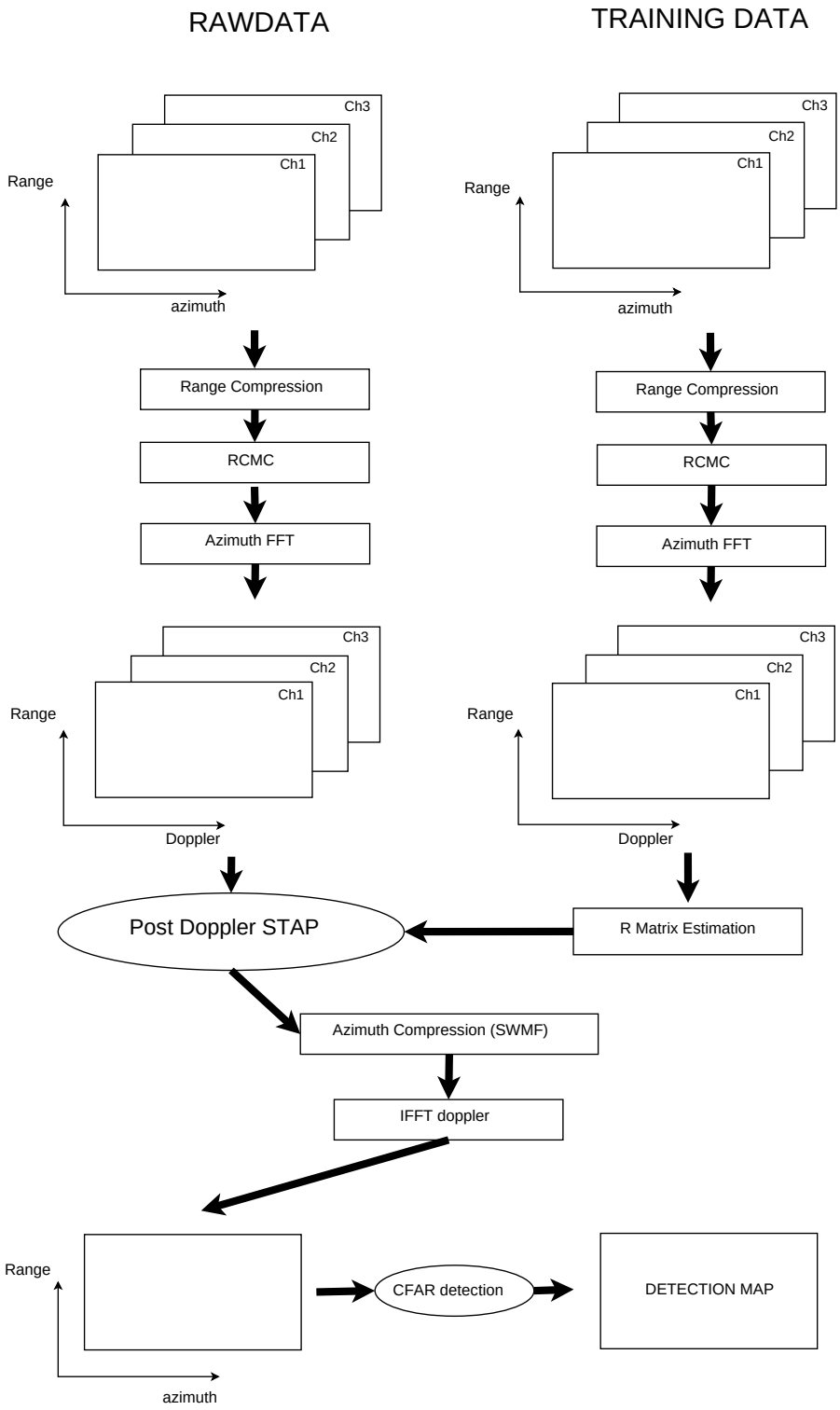

Figure 3.1: Detection Algorithm

3.2.1 Constant False Alarm Rate Detector

In radar detection is always desirable to have a constant rate of false alarms in the detection, to do so is necessary to know the statistics of the noise+clutter after the whole processing. This permits to choose a threshold that allows a constant

false alarm detection CFAR.

Under the assumption of complex gaussian model for the clutter and noise, and considering that the SAR operations in the process chain (range and azimuth compression, STAP, RCMC) are linear processes the statistical model of clutter and noise at the end of the process will be also gaussian.

So under this assumption of complex gaussian model for the clutter and noise it turns out that the probability density function (pdf) of the magnitude is Rayleigh.

$$f(x,\sigma) = \frac{x}{\sigma^2} e^{\frac{x^2}{2\sigma}} \tag{3.8}$$

where x is the magnitude and σ is the rayleigh parameter. In this case the threshold could be found using the theoretical cumulative distribution function of the rayleigh distribution:

$$th = \sqrt{-\log(p_{fa}) 2\sigma^2} \tag{3.9}$$

where p_{fa} is the imposed probability of false alarm. To validate this hypothesis the clutter+noise statistics has been computed and compared to a rayleigh approximation for the three different clutter scenario that will be used in the simulations to model the sea clutter:

- $\sigma_0 = -25dB$, decorrelation time $\tau_c = 60ms$
- $\sigma_0 = -15dB$, decorrelation time $\tau_c = 32ms$
- $\sigma_0 = -12dB$, decorrelation time $\tau_c = 31ms$

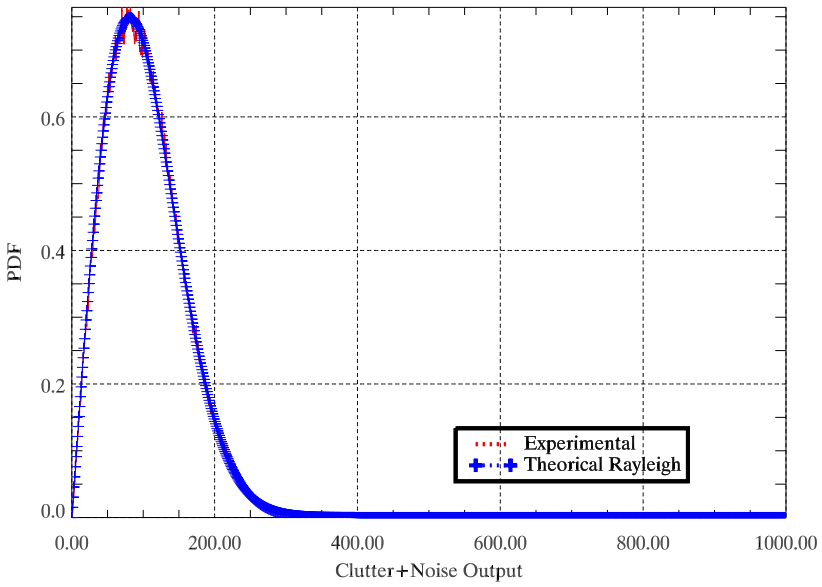

Figure 3.2: Comparison of the experimental Noise+Clutter PDF with a rayleigh approximated PDF for clutter ($\sigma_0 = -25dB$, $\tau_c = 60ms$)

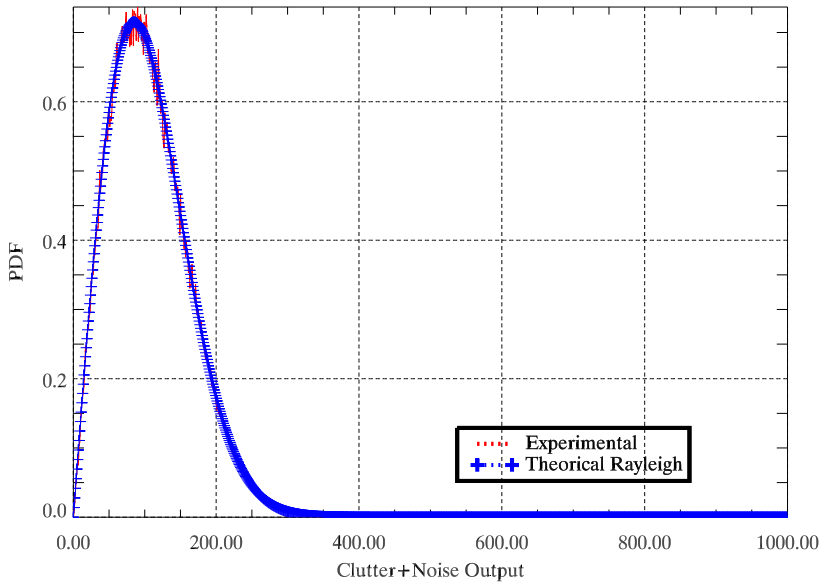

Figure 3.3: Comparison of the experimental Noise+Clutter PDF with a rayleigh approximated PDF for clutter ($\sigma_0 = -15dB$, $\tau_c = 32ms$)

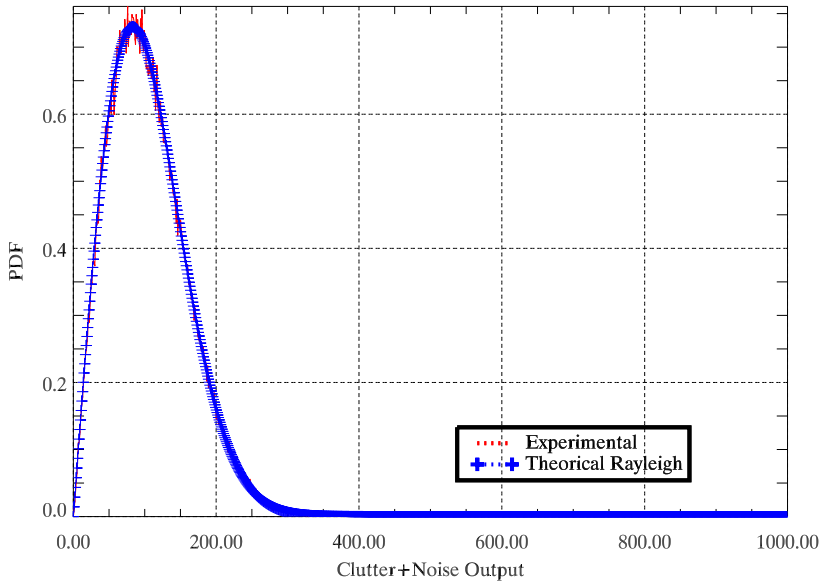

Figure 3.4: Comparison of the experimental Noise+Clutter PDF with a rayleigh approximated PDF for clutter ($\sigma_0 = -12dB$, $\tau_c = 31ms$)

As the images clearly show the rayleigh approximation holds. This allows the calculation of the threshold as indicated in 3.9, where the rayleigh parameter is estimated as follows:

$$\sigma = \sqrt{\frac{\sum_{i=1}^{n-1} x_i}{2n}} \tag{3.10}$$

3.3 Along-Track velocity Estimation

The along-track velocity component of a moving vehicle can be derived indirectly by processing SAR data with varying frequency modulation (FM) rates and exploiting the specific behavior of the vehicle's signal through the FM rate space [13].

In SAR processing the vehicles moving in along-track appear smeared in azimuth direction, when nominal SAR azimuth focusing (SWMF) is performed. Along-track motion changes the relative velocity of sensor and vehicle resulting in a change of the FM rate and consequently in a mismatch of the vehicle's signal and the Stationary Word Matched Filter. The extent of this defocusing is directly proportional to the along track velocity of the target.

Re-sharpening of defocused moving targets in SAR images is achieved by varying the FM rate of the matched filter. This allows estimating indirectly the along-track velocity component of the vehicle

In our case, the maximization of the peak energy in done not only varying the FM rate of the matched filter but also performing a post-Doppler STAP processing with a steering vector adapted to the along-track velocity under test.

Chapter 4

Simulation Results

The simulations has been performed with the parameters of the future SEOSAR/-PAZ mission [7] that's the first Spanish Satellite based on the use of a high resolution X-band Synthetic Aperture Radar (SAR). The versatility of the PAZ SAR instrument provides the possibility to exploit a series of experimental applications using the Dual Receive Antenna mode. In table 4.2 SEOSAR/PAZ mission parameters are reported.

Figure 4.1: A rendering of the PAZ satellite

Orbit height	510 Km
Radar frequency	9.65 Ghz
Antenna dimensions	4.8m (lenght) by 0.7 m (height)
BW of trasmitted signal	75 MHz
Sampling frequency	110 MHz
PRF	3.92 KHz
Noise Temperature	790K

Table 4.1: Parameters of SEOSAR/PAZ mission.

4.1 Simulated Scenario

The simulations has been run over a 1km×1km sea scenario, to simulate the sea clutter the mean reflectivity coefficient σ_0 for the gaussian distribution has been extrapolated in the table compiled by Nathanson et al. in [5]. The temporal decorrelation parameter τ_c is chosen according to the temporal decorrelation of the sea surface [6] by the approximation:

$$\tau_c \cong 3\frac{\lambda}{u} erf^{-1/2}\left(2,7\frac{x}{u^2}\right) \ , \tag{4.1}$$

where u is the wind speed, x is the spatial resolution in ground range and $erf()$ is the Gauss error function. The sea specifications are in agreement to the World Meteorological Organization sea state code [15] and the Beaufort wind scale [15].

Sea State	wind speed $[\frac{m}{s}]$	σ_0 [dB]	decorrelation time τ_c [ms]
0	1	-25	60
4	10	-15	32
6	16	-12	31

Table 4.2: Characteristics of the sea clutter model used in the simulations

The Radar Cross Section of the moving targets used in the simulations has been chosen according to [12] in order to simulate the RCS of different types of boat:

0**dBsm** to simulate the echo return from of a small boat, like a speedboat (8m (length) x 2m (wide)).

10**dBsm** to simulate the echo return of a medium size boat, like a small fishing boat (15m (length) x 5m (wide)).

20**dBsm** to simulate the echo return of a big fishing vessel (60m (length) x 10m (wide)).

30**dBsm** to simulate the echo return of a ferry boat (100m (length) x 20m (wide)).

The simulation of a real echo return of a boat is not in the objective of this project and is generally very complicated, in the simulation a single point target approximation has been used. The velocity range considered for the simulation has been chosen coherently to the field of application, in this case a marine scenario with moving boats, so both the range of velocity has been limited to $[-15,\ldots,+15]\frac{m}{s}$.

4.2 DRA results

The first mode of operation used the simulation has been the Dual Receive Antenna. Before starting with the simulation of the moving target the three different clutter scenario has been simulated and processed in order to estimate the

threshold to be applied in the detection and the efficacy of the STAP in the clutter reduction. Two different type of steering vector have been used in the STAP algorithm, the first one is the steering vector described in which is adapted to a specifical target velocity, the second one is a fixed steering vector $\mathbf{a} = [1 - 1]$ that's a sub-optimal solution to the problem proposed by Klemm in [11].

4.2.1 CNR

The Clutter to Noise Ratio has been evaluated in the range-Doppler domain before and after the STAP process, in table 4.4 the results for the the three clutter scenario are reported in the case of the STAP with adapted steering. It is possible to see how in this case the STAP filtering cannot reduce the clutter below the noise level while in the case of the STAP with steering [1 -1] the clutter is attenuated below the noise level as can be noted in table **??**.

Sea state	CNR before STAP [dB]	CNR after STAP [dB]	CNR gain [dB]
0	-2	-2.5	0.5
4	8	-0.2	8.2
6	11	-0.8	11.8

Table 4.3: DRA: CNR before and after STAP processing for adapted steering

Sea state	CNR before STAP [dB]	CNR after STAP [dB]	CNR gain [dB]
1	-2	-22.7	20.7
2	8	-12.1	20.1
3	11	-13.3	22.3

Table 4.4: DRA: CNR before and after STAP processing for [1 -1] steering

4.2.2 SCNR

The Signal to Clutter and Noise Ratio after the processing it's a very important parameter to evaluate the performance of a processing because the detection probability depends on it. The SCNR has been evaluated for the sea state 4 clutter and for two different possibilities:

- Target moving only with Across-Track velocity
- Target moving only with Along-Track velocity

The graphics 4.2 shows the behaviors of the STAP processing (in terms of SNCR) respect to moving targets with only across-track velocity; the shape of the SCNR curve for the adapted steering STAP has no attenuation for the $v_{across} = 0$

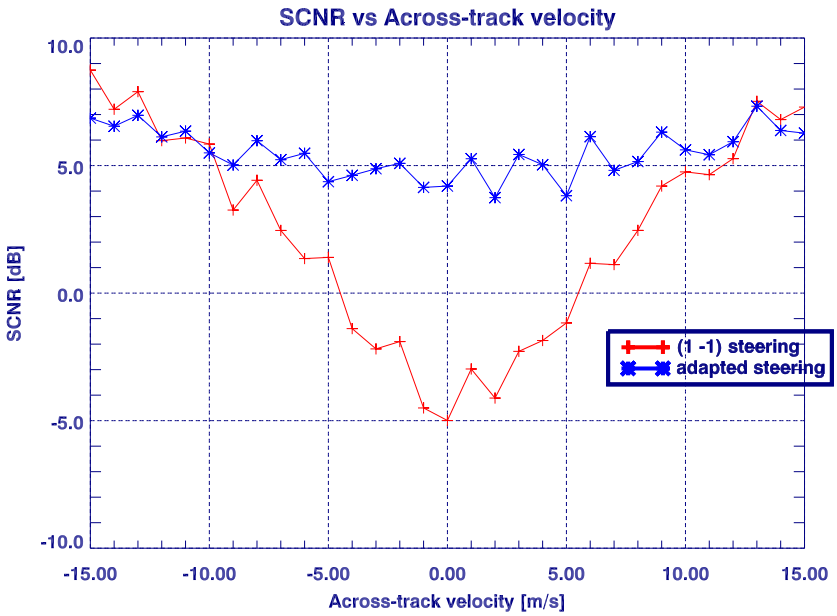

Figure 4.2: DRA: SCNR as a function of Across-Track velocity for a $0dBm^2$ RCS target

respect to the moving targets. On the other hand the application of the $[1, -1]$ steering vector produce a more accentuated notch for velocities in the proximity of zero.

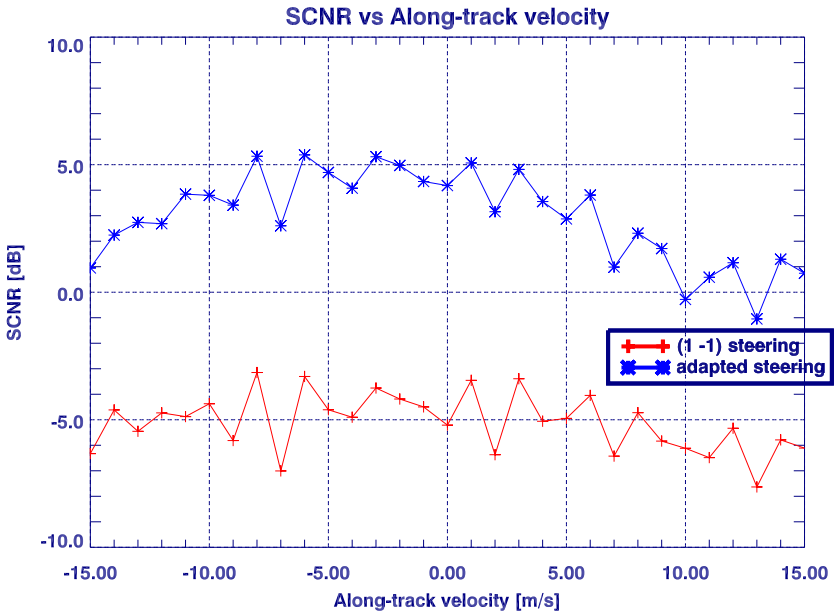

Figure 4.3: DRA: SCNR as a function of Along-Track velocity for a $0dBsm$ RCS target

The behaviors of the STAP processing respect to the along-track velocity are shown in fig 4.3,the SCNR has its maximum for target velocities close to zero and decreases as the velocity increases. This behavior appears to be dependent on the application of a SWMF for the compression after the STAP that causes defocusing

of the target with v_{along} different from zero and a consequent magnitude reduction. The application of the $[1, -1]$ steering vector produce a similar shape of the curve but placed almost $10dB$ below.

4.2.3 Detection Probability

The detection probability has been evaluated over only the positive range of velocities $[1, \ldots, 15]\frac{m}{s}$ because of the similar behavior of the SCNR for the negative velocities respect to the positive ones. The probability of false alarm has been fixed to $p_{fa} = 10^{-5}$ which is a usual choice in radar systems. The evaluation of the Pd has been made over 30 trials.

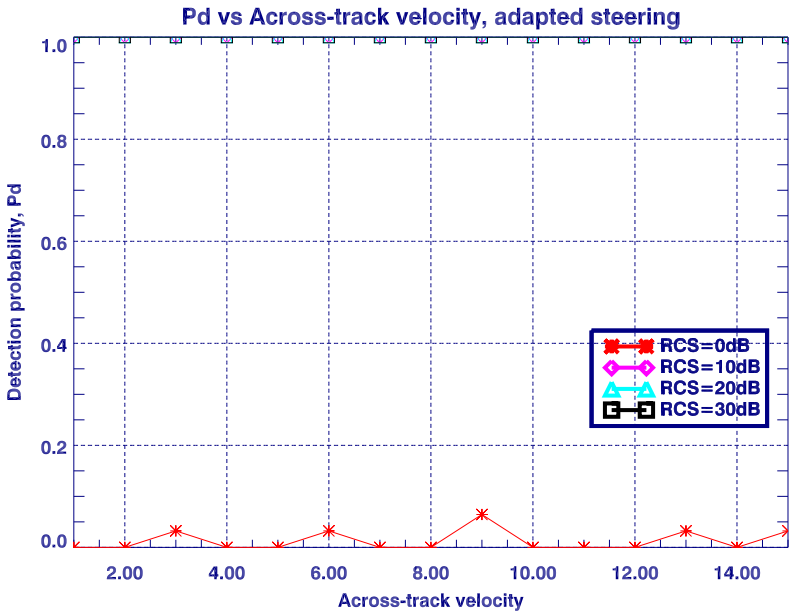

Figure 4.4: DRA: Pd as a function of Across-Track velocity for different RCS, Adapted Steering

As shown in figure 4.4 in case of Across-Track only moving target processed with the steering adapted to the target velocity, for RCS $10dBsm, 20dBsm, 30dBsm$ the target is detected for all the velocities, whereas for $0dBsm$ RCS the target is detected in just a few trials over the total amount.

If the $[1 - 1]$ steering vector is applied (fig 4.5) in the STAP processing then only the target with $20dBsm, 30dBsm$ of RCS are detected independently of their velocities, the $10dBsm$ RCS target is detected with a probability that increases as the velocity increases and the $0dBsm$ RCS one is poorly detected only for high velocities.

In the case of Along-Track velocity with adapted steering (fig 4.6), again the $10dBsm, 20dBsm$ RCS targets are detected for every velocity in the range, the $10dBsm$ is detected with higher probability for small velocities and the $0dBsm$ is never detected. For the $[1 - 1]$ steering case the $30dBsm, 20dBsm$ RCS targets are always detected whereas the $10dBsm, 0dBsm$ ones are nearly never detected.

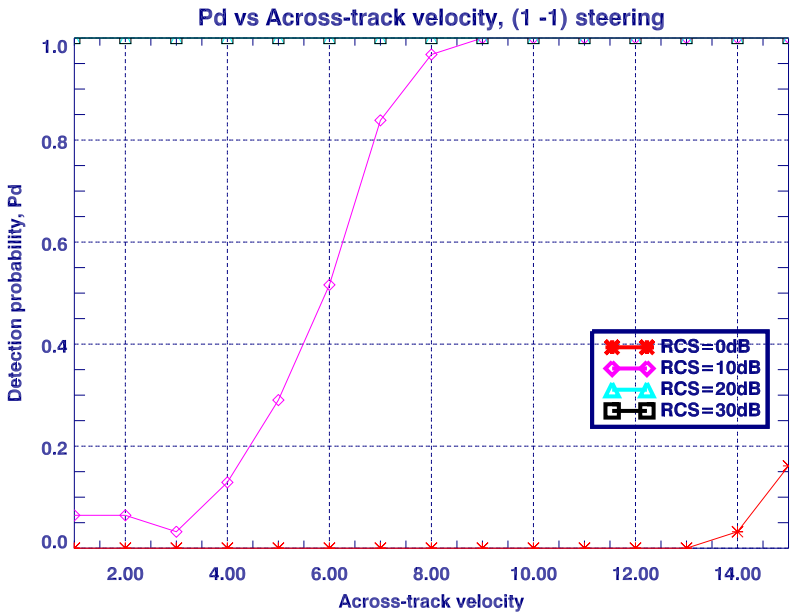

Figure 4.5: DRA: Pd as a function of Across-Track velocity for different RCS, $[1 - 1]$ Steering

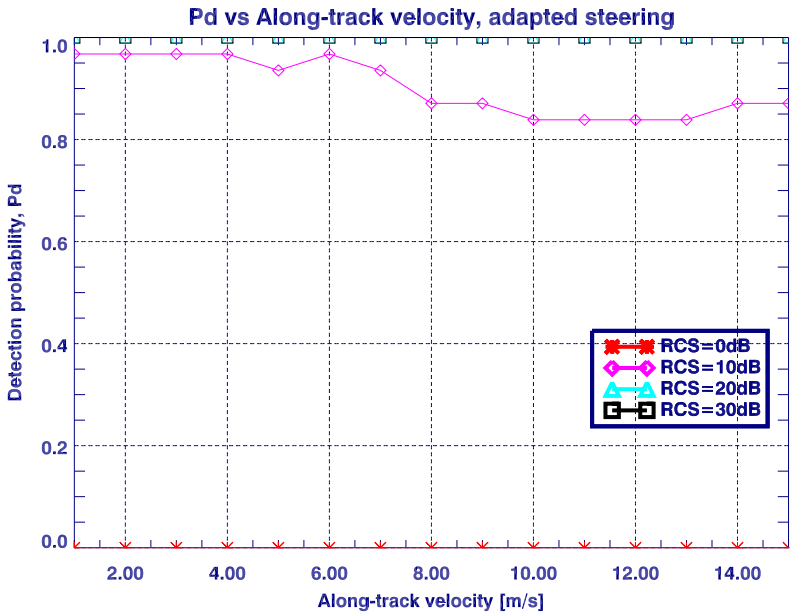

Figure 4.6: DRA: Pd as a function of Along-Track velocity for different RCS, Adapted Steering

In figures 4.8 and 4.9 are shown the probability of detection for target having the both velocity components across and along different from zero. The graphics shows how the detection probability of a target are strongly concatenated to its across-track velocity especially in the $[1 - 1]$ steering case.

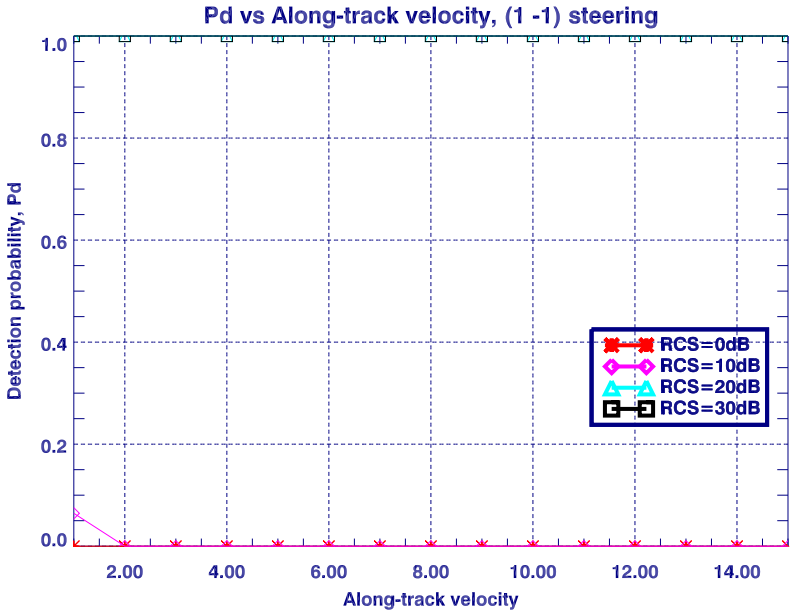

Figure 4.7: DRA: Pd as a function of Along-Track velocity for different RCS, $[1-1]$ Steering

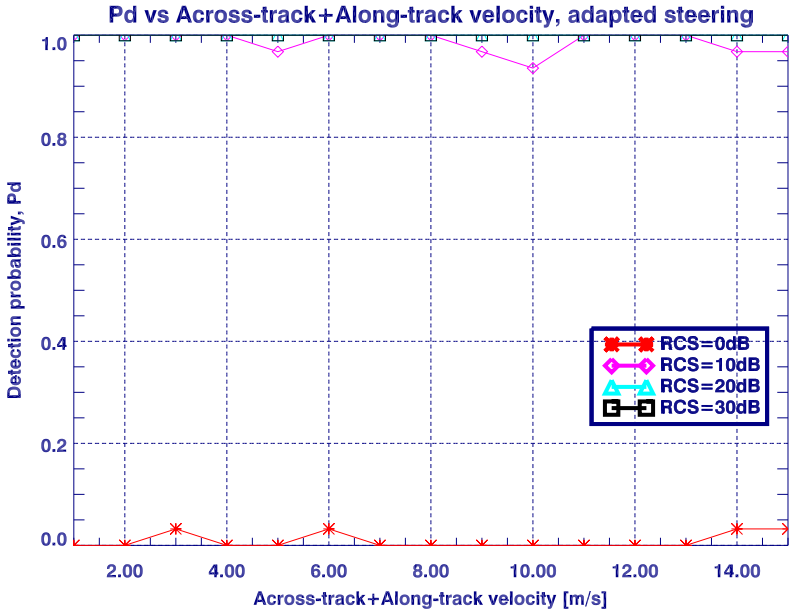

Figure 4.8: DRA: Pd as a function of Along+Across-Track velocity for different RCS, Adapted Steering

4.2.4 Along-Track velocity estimation

The estimation of the Along-Track velocity is indirectly made, once a target has been detected, using a bank of azimuth matched filter to azimuth line in which the target has been detected for a finite number of possible velocities. The estimated along-track velocity is the one that maximize output. In the estimation algorithm the range of tested along-track velocities has been fixed as $[-25,\ldots,+25]\frac{m}{s}$.

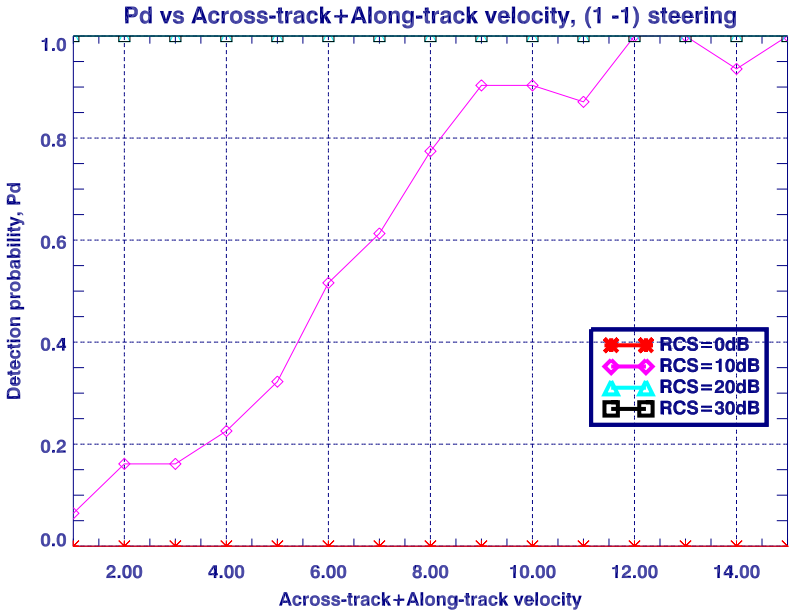

Figure 4.9: DRA: Pd as a function of Along+Across-Track velocity for different RCS, $[1-1]$ Steering

Two significative case are showed, in the first one a $20dBsm$ RCS target moving with $v_{across} = v_{along} = 3\frac{m}{s}$ is processed whereas in the second a target with the same RCS but $v_{across} = v_{along} = 11\frac{m}{s}$ is processed.

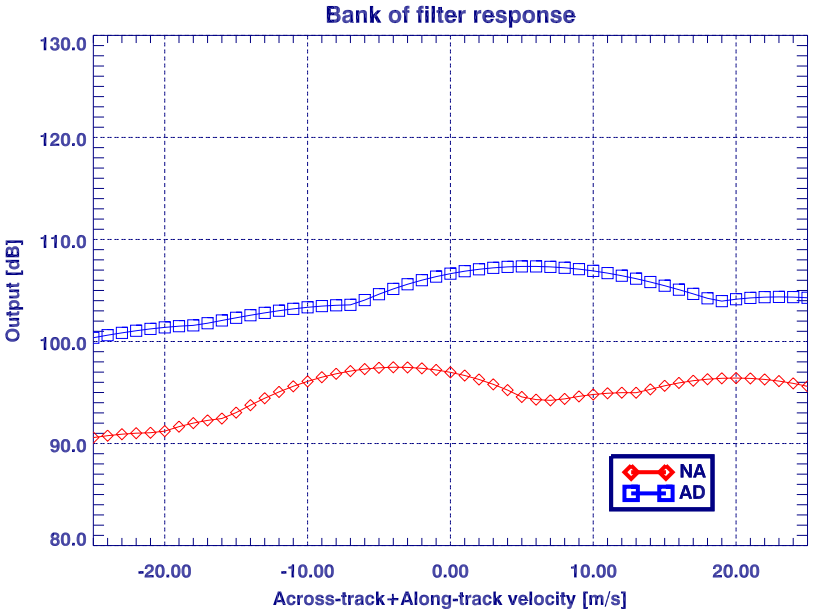

Figure 4.10: DRA: Bank of filter OUTPUT for a $3\frac{m}{s}$ along-track moving target $20dBsm$ RCS

In the first case (4.10) the velocity estimated applying a adapted steering vector ($\hat{v}_{along} = 5\frac{m}{s}$)is clearly much more reliable respect to the one estimated with the

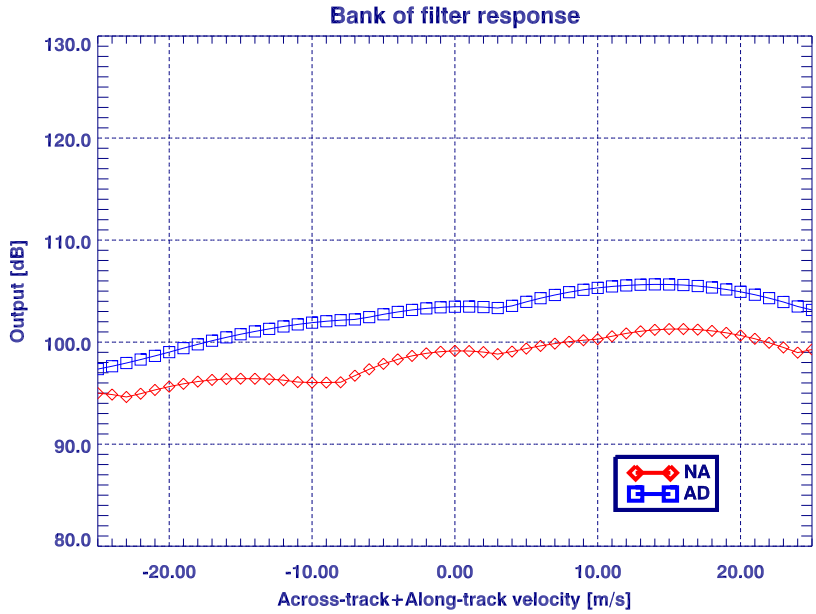

Figure 4.11: DRA: Bank of filter OUTPUT for a $12\frac{m}{s}$ along-track moving target $20dBsm$ RCS

$[1 - 1]$ steering vector ($\hat{v}_{along} = -4\frac{m}{s}$) in the STAP process. In the second case (4.11)instead the two estimated velocity are both reliable ($\hat{v}_{along} = 12\frac{m}{s}$ for the adapted steering, $\hat{v}_{along} = 15\frac{m}{s}$ for [1 -1] steering).

A complete table of the estimated velocity for different moving target could be found in 4.5.

4.3 TOGGLE modes results

In chapter two the possibility to generate an additional channel by exploiting the flexibility in the programming of the radar antenna has been introduced. The three virtual channels toggle receive mode has been implemented in the simulator and its performances has been evaluated.

4.3.1 CNR

The Clutter to Noise Ratio has been evaluated in the range-Doppler domain before and after the STAP process, in table 4.6 the results for the the three clutter scenario are reported for STAP with adapted steering. It is possible to see how in this case the STAP filtering cannot reduce the clutter below the noise level as was in the DRA case.

4.3.2 SCNR

Figure 4.12 shows the behaviors of the STAP processing with adapted steering respect to the across-track velocity, as in the DRA the static target with $v_{across} = 0$

$v_{along}[\frac{m}{s}]$	$\hat{v}_{along}[\frac{m}{s}]$ ad. st.	error $[\frac{m}{s}]$	$\hat{v}_{along}[\frac{m}{s}]$ [1 -1] st.	error $[\frac{m}{s}]$
-15	-17	2	-12	3
-14	-16	2	-16	2
-13	-9	4	-15	2
-12	-13	1	-15	3
-11	-13	2	-13	2
-10	-12	2	-13	3
-9	-12	3	-12	3
-8	-7	1	-13	5
-7	-8	1	-11	4
-6	-7	1	-8	2
-5	-2	3	-9	4
-4	-1	3	-9	5
-3	-3	0	$+1$	4
-2	0	2	3	5
-1	$+2$	3	-4	3
0	$+1$	1	-4	4
$+1$	$+3$	2	-4	5
$+2$	$+4$	2	-5	7
$+3$	$+5$	2	-4	7
$+4$	$+7$	3	-1	5
$+5$	$+4$	1	$+2$	3
$+6$	$+4$	2	$+1$	5
$+7$	$+5$	2	$+4$	3
$+8$	$+7$	1	$+4$	4
$+9$	$+10$	1	$+7$	2
$+10$	$+12$	2	$+9$	1
$+11$	$+14$	3	$+13$	2
$+12$	$+13$	1	$+15$	3
$+13$	$+11$	2	$+16$	3
$+14$	$+12$	2	$+12$	2
$+15$	$+14$	1	$+13$	2

Table 4.5: DRA: estimated along track velocity for $20dBsm$ RCS target

Sea state	CNR before STAP [dB]	CNR after STAP [dB]	CNR gain [dB]
1	-5	-5.2	0.5
2	5	-0.7	4.3
3	8	-0.3	7.7

Table 4.6: TOGGLE: CNR before and after STAP processing for adapted steering

is not strongly attenuated by the STAP respect to the the targets with higher v_{across}.

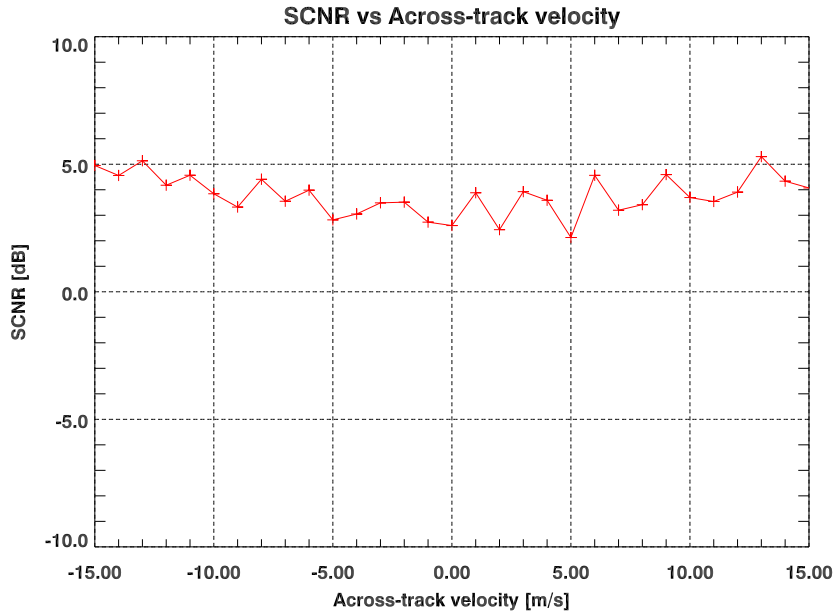

Figure 4.12: TOGGLE: SCNR as a function of Across-Track velocity for a $0dBsm$ RCS target

It can be noted that in along-track velocity (fig 4.13) the SCNR has its maximum for target velocities close to zero and decreases as the velocity increases. This behavior appears to be dependent on the application of a SWMF for the compression after the STAP that causes defocusing of the target with v_{across} different from zero and a consequent magnitude reduction.

4.3.3 Detection Probability

As in the DRA the detection probability has been evaluated over only the positive range of velocities $[1, \ldots, 15]\frac{m}{s}$ because of the similar behavior of the SCNR for the negative velocities respect to the positive ones. The probability of false alarm has been fixed to $p_{fa} = 10^{-5}$. The evaluation of the Pd has been evaluated over 30 trials.

In the case of moving target with only across-track velocity (fig 4.14), processed with the adapted steering vector, for RCS $20dBsm, 30dBsm$ the target is detected for all the velocities, for $20dBsm$ RCS the estimated probability is very close to one, whereas for $0dBsm$ RCS the target is detected in just a few trials over the total amount.

In the case of Along-Track velocity with adapted steering (fig 4.15), again the $30dBsm, 20dBsm$ RCS targets are detected for every velocity in the range, the $10dBsm$ target detection probability decreases as the velocity increases,the $0dBsm$ RCS target is never detected.

Finally in figure 4.16 the probability of detection has been evaluated for target having the both velocity components across and along different from zero. In this

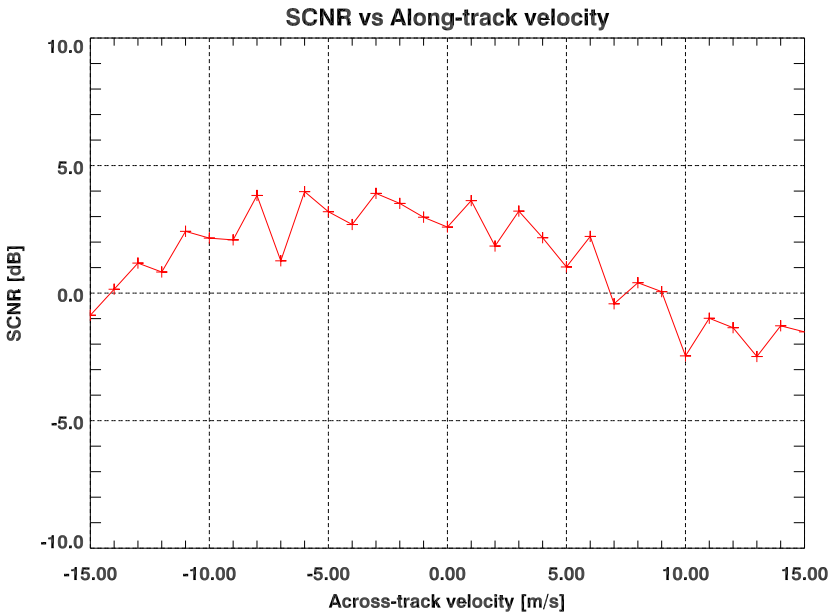

Figure 4.13: TOGGLE: SCNR as a function of Along-Track velocity for a $0dBsm$ RCS target

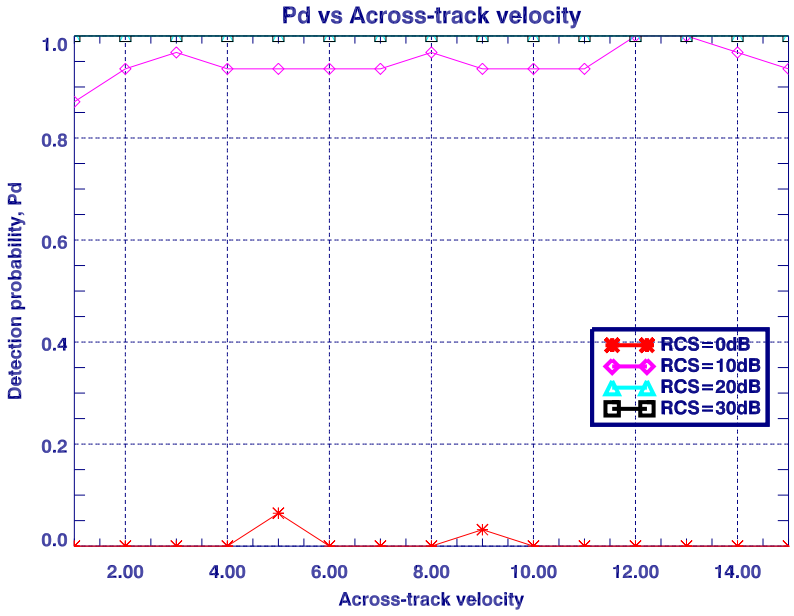

Figure 4.14: TOGGLE: Pd as a function of Across-Track velocity for different RCS

case the defocusing effect due to the along-track velocity (as seen in the SCNR) seems to be dominant for velocities until $10\frac{m}{s}$ then the effects of across-track velocity becomes dominant.

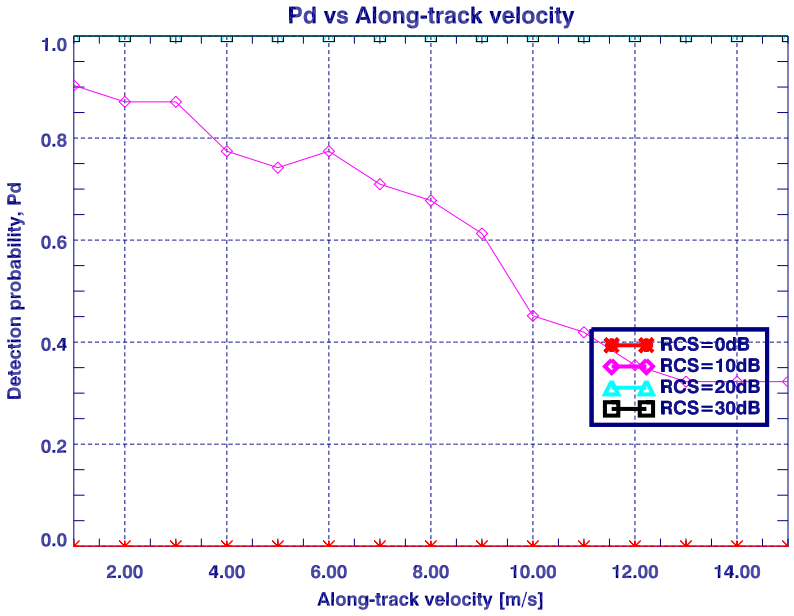

Figure 4.15: TOGGLE: Pd as a function of Along-Track velocity for different RCS

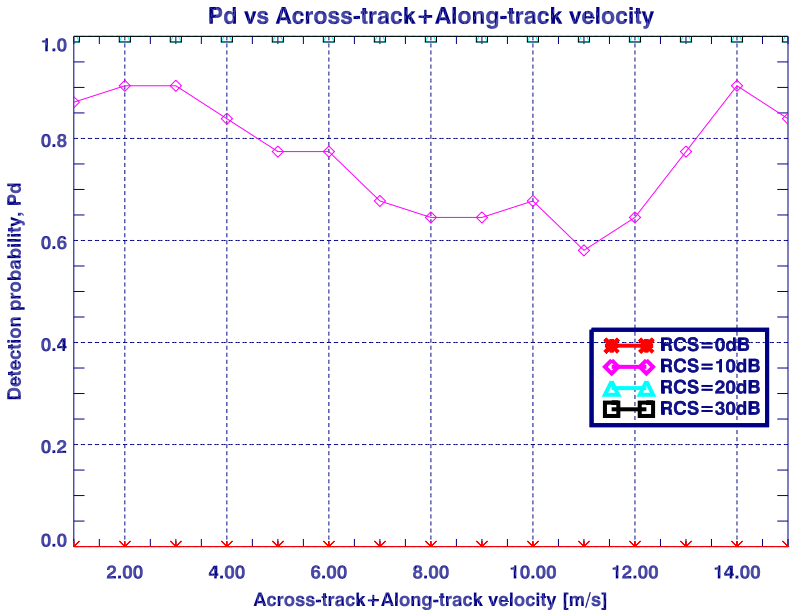

Figure 4.16: TOGGLE: Pd as a function of Along+Across-Track velocity for different RCS

4.3.4 Along-Track velocity estimation

As for the DRA, two significative cases are showed (fig 4.17 and fig 4.18), in the first one a $20dBsm$ RCS target moving with $v_{across} = v_{along} = 3\frac{m}{s}$ is processed whereas in the second a target with the same RCS but $v_{across} = v_{along} = 11\frac{m}{s}$ is processed.

In the first case the estimated along-track velocity is $\hat{v}_{along} = 6\frac{m}{s}$) In the second case instead the estimated along-track velocity is ($\hat{v}_{along} = 15\frac{m}{s}$

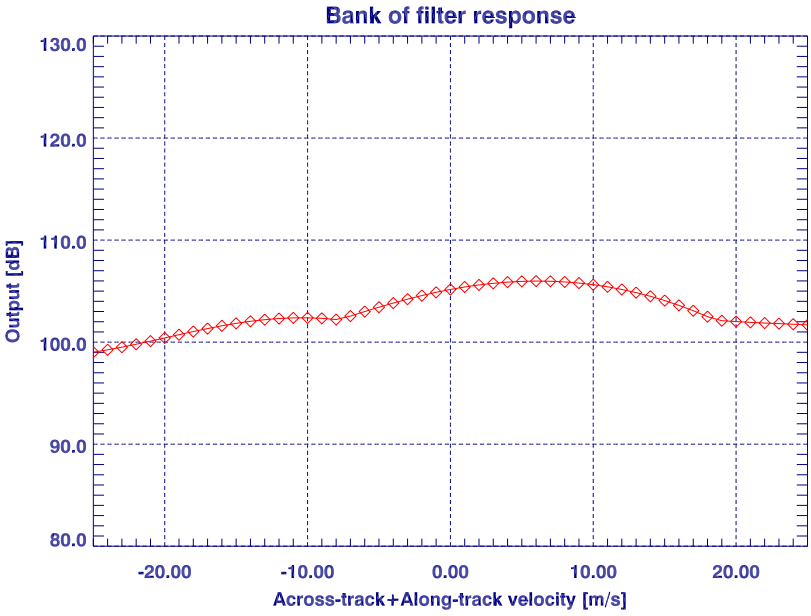

Figure 4.17: TOGGLE: Bank of filter OUTPUT for a $3\frac{m}{s}$ along-track moving target $20dBsm$ RCS

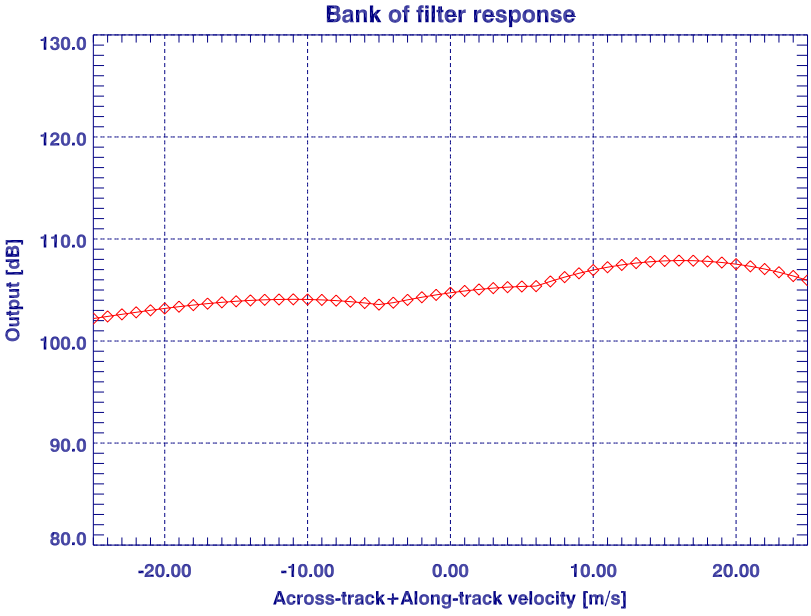

Figure 4.18: TOGGLE: Bank of filter OUTPUT for a $12\frac{m}{s}$ along-track moving target $20dBsm$ RCS

A complete table of the estimated velocity for different moving targets could be found in 4.7.

$v_{along}[\frac{m}{s}]$	$\hat{v}_{along}[\frac{m}{s}]$ ad. st.	error $[\frac{m}{s}]$
-15	-16	1
-14	-17	3
-13	-11	2
-12	-13	1
-11	-14	3
-10	-12	2
-9	-12	3
-8	-7	1
-7	-9	2
-6	-7	1
-5	-2	3
-4	-2	2
-3	-3	0
-2	0	2
-1	$+2$	3
0	$+1$	1
$+1$	$+3$	2
$+2$	$+5$	3
$+3$	$+6$	3
$+4$	$+6$	2
$+5$	$+7$	2
$+6$	$+4$	2
$+7$	$+10$	3
$+8$	$+7$	1
$+9$	$+12$	3
$+10$	$+12$	2
$+11$	$+15$	4
$+12$	$+13$	1
$+13$	$+11$	2
$+14$	$+12$	2
$+15$	$+14$	1

Table 4.7: TOGGLE: estimated along track velocity for $20dBsm$ RCS target

4.4 Analysis of the results

From the SCNR results appears clear that, for the simulated marine clutter scenario, the application of the STAP with the adapted steering vector don't give an attenuation for the static target as would be desiderate in GMTI.

Experimental investigations has demonstrated that the cause of the problem relies on the small Clutter-Noise-Ratio of $15dB$ of the simulated scenario in the range-Doppler domain at the moment of estimation of the spectral power density matrix $\mathbf{R}$.

In figure 4.19 the SNCR after the processing for a target with only across-track velocity and for 2 different clutter backscatter coefficient ($\sigma_0 = 0dB$ and $\sigma_0 = 10dB$), providing respectively a CNR improvement of $15dB$ and $20dB$, is shown. Appears evident how the STAP filtering in this case is strongly attenuating the echoes from the static target.

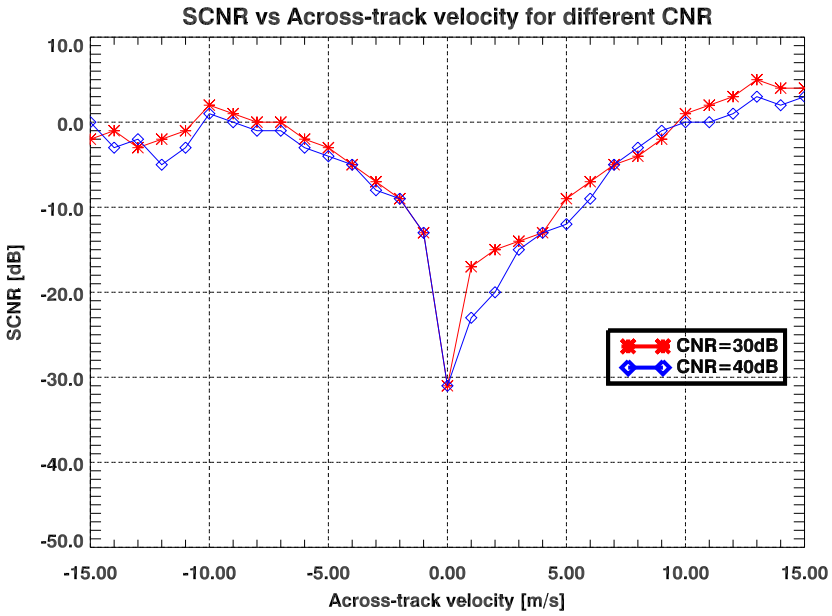

Figure 4.19: DRA, SCNR as a function of Across-Track velocity for a $0dBsm$ RCS target, different CNR

The results with the TOGGLE mode of operation are even better than what found for the DRA in terms of attenuation of the static target as fig 4.20 shows.

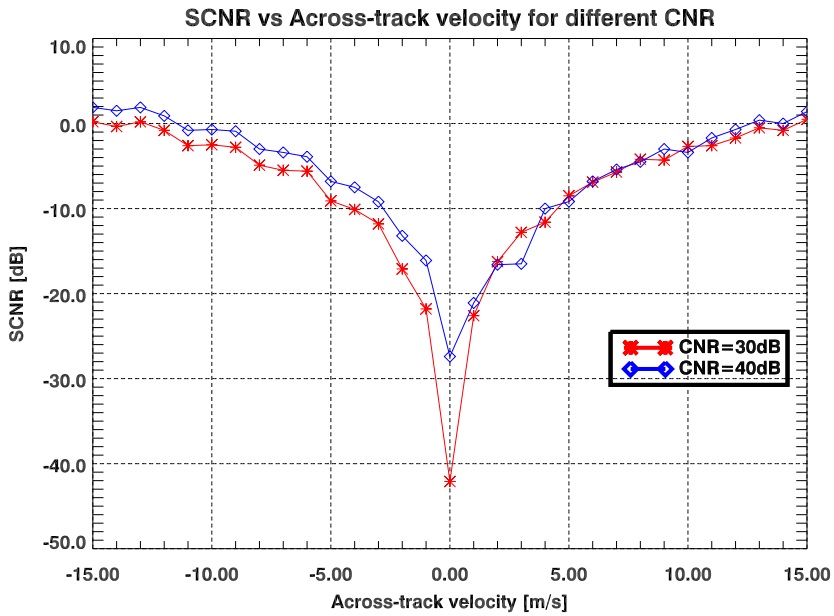

Figure 4.20: SCNR as a function of Across-Track velocity for a $0dBsm$ RCS target

Chapter 5

Conclusions and future work

A post-Doppler STAP processing technique has been implemented and integrated in the SAR processing for detection of moving targets in maritime scenario. The performance of such technique has been evaluated with the integration of the algorithm in the SAR-GMTI simulator developed in the Department of Signal Theory and Communications (TSC). In simulation of the spaceborne SAR the parameters of the future Spanish PAZ mission have been used. Two different mode of operation have been considered, the Dual Receive Antenna (DRA) that allows the creation of two channel and a TOGGLE mode of operation that makes possible the creation of an additional channel by doubling the pulse repetition frequency (PRF) and exploiting the flexibility in programming the array antenna. The performance of the implemented technique has been evaluated in a maritime scenario and with the simulation of four different types of boats.

In the DRA mode of operation, two different choice of steering vector in the post-Doppler STAP have been used, the results obtained in the application of the technique to a marine clutter scenario have shown that a clutter reduction is provided by both possible choice of steering vector. For the adapted steering case the reduction of the clutter is lower respect the [1 -1] steering vector. In the TOGGLE mode of operation just the adapted steering vector has been considered (as the [1 -1] steering vector can only be applied with two channels) and a clutter reduction has been obtained.

The SCNR in the case of post-Doppler STAP with adapted steering is higher than the one obtained with the [1 -1] steering and allows a better detection of the moving targets.

In the case of a static point-like target the results have shown that a better CNR (respect to the one in the simulated maritime scenario) is required in order to cancel it with the post-Doppler STAP.

The simulations have shown better detection probability in the case of adapted steering vector, of particular interest is the detection probability results obtained for moving targets with only along-track velocity, since generally with DPCA or ATI processing techniques they are almost impossible to detect.

The along-track velocity estimation is better performed in the case of adapted steering with a maximum error of $4\frac{m}{s}$.

The results obtained with the TOGGLE mode of operation have shown no appreciable improvements respect the DRA mode for the simulated scenarios.

The future work in this field should be addressed in the study of a more realistic model for maritime clutter and in the creation of more detailed models of the different type of boats in order to estimate in a better way the performance of the proposed technique.

Bibliography

[1] S. Barbarossa and A. Farina. "Space-time-frequency processing of synthetic aperture radar signals". In: *Aerospace and Electronic Systems, IEEE Transactions on* 30.2 (1994), pp. 341 –358.

[2] D. Cerrutti-Maori and I. Sikaneta. "Optimum GMTI Processing for Space-based SAR/GMTI Systems -Theoretical Derivation-". In: *Proceedings of EUSAR* (2010).

[3] J.H.G. Ender. "Space-time-frequency processing of synthetic aperture radar signals". In: *Electronics and Communication engineering jurnal* (1999), pp. 29 –38.

[4] J.H.G. Ender, C.H. Gierull, and D. Cerutti-Maori. "Improved Space-Based Moving Target Indication via Alternate Transmission and Receiver Switching". In: *Geoscience and Remote Sensing, IEEE Transactions on* 46.12 (2008), pp. 3960 –3974.

[5] M. Cohen F. Nathanson J. Reilly. *Radar Design Principles - Signal Processing and the Environment*. SciTech Pub, 1999, Sea clutter table 134 –147.

[6] S.J. Frasier and A.J. Camps. "Dual-beam interferometry for ocean surface current vector mapping". In: *Geoscience and Remote Sensing, IEEE Transactions on* 39.2 (2001), pp. 401 –414.

[7] A.S. Gonzalez et al. "PAZ instrument design and performance". In: *Synthetic Aperture Radar (APSAR), 2011 3rd International Asia-Pacific Conference on*. 2011, pp. 1 –4.

[8] J. Guerci. *Space-Time Adaptive Processing for Radar*. Artech House, USA, 2003.

[9] Frank H. Wong Ian G. Cumming. *Digital Processing of Synthetic Aperture Radar Data: Algorithms and Implementation*. Artech House Publishers, 2005.

[10] R. Klemm. "Introduction to space-time adaptive processing". In: *Electronics and Communication engineering jurnal* (1999).

[11] R. Klemm. *Principles of Space-Time Adaptive Processing*. IEE Publisher, London UK, 2002.

[12] Gonzales O. Makhoul E. Broquetas E. "Evaluation of State-of-the-Art techniques for Future Spaceborne SAR system -Simulation Validation-". In: (2011).

[13] G. Palubinskas et al. "Estimation of along-track velocity of road vehicles in SAR data". In: *Image and Signal Processing for Remote Sensing XI*. 2005.

[14] J.J. Sharma, C.H. Gierull, and M.J. Collins. "The influence of target acceleration on velocity estimation in dual-channel SAR-GMTI". In: *Geoscience and Remote Sensing, IEEE Transactions on* 44.1 (2006), pp. 134 –147.

[15] *World Meteorological Organization Manual on Codes, No 306*. URL: http://www.wmo.int/pag